ISSN 1023-1935, Russian Journal of Electrochemistry, 2016, Vol. 52, No. 3, pp. 193–219. © Pleiades Publishing, Ltd., 2016.
Original Russian Text © M.R. Tarasevich, E.S. Davydova, 2016, published in Elektrokhimiya, 2016, Vol. 52, No. 3, pp. 227–256.

Nonplatinum Cathodic Catalysts for Fuel Cells with Alkaline Electrolyte (Review)

M. R. Tarasevich and E. S. Davydova*

Frumkin Institute of Physical Chemistry and Electrochemistry, Russian Academy of Sciences, Leninskii pr. 31, Moscow, 119991 Russia

**e-mail: elena.s.davydova@yandex.ru*

Received March 18, 2015

Abstract—The review is devoted to the analysis of the state-of-the-art in the development of highly dispersed non-platinum catalysts of O_2 electroreduction and their use in cathodes of alkaline fuel cell. Attention is focused on the development of catalysts for fuel cells with anion-exchange membrane. The range of catalytic materials under consideration includes complex oxides, unmodified carbon materials and also carbon materials doped with a transition metal and/or nitrogen. The main synthetic methods for nanodispersed catalysts are considered, particularly those used for synthesizing new types of N-doped carbon materials. A comparative description of peculiarities of O_2 reduction on different groups of catalysts is carried out. The possible nature of catalytically active centers is discussed. The problems of further studies on the development of nonplatinum catalysts for fuel-cells cathodes with anion-exchange membranes are formulated.

Keywords: fuel cell, alkaline medium, oxygen reduction, nonplatinum catalyst, carbon material, doping, active center, RRDE

DOI: 10.1134/S1023193516030113

1. INTRODUCTION

To date, the most thoroughly developed and commercially promising fuel cell (FC) types are those with proton-exchange membrane electrolyte (PEM). A considerable number of such FC are already produced for both stationary and transport applications. However, their commercial production is limited by their high cost, first of all, due to the necessity of using considerable amounts of Pt as the catalyst, especially, on the cathode for attaining their reasonable durability [1]. Moreover, platinum is the only FC component the cost of which does not decrease with the increase in the production of electrochemical generators (ECG). This fundamental drawback of FC with PEM is not the case for alkaline FC (AFC) as their production and operation can succesfully manage without the use of platinum or other noble metals.

The modern history of the development of fuel cells began with the studies of alkaline fuel cells [2], because sufficiently high ECG power values had been achieved for this very system. AFC were successfully used in the US space program [2] and have been actively developed in the 60s–70s by the company Kvant [3] and further up to present time by the company "Zavod Elektrokhimicheskikh Preobrazovatelei." In the

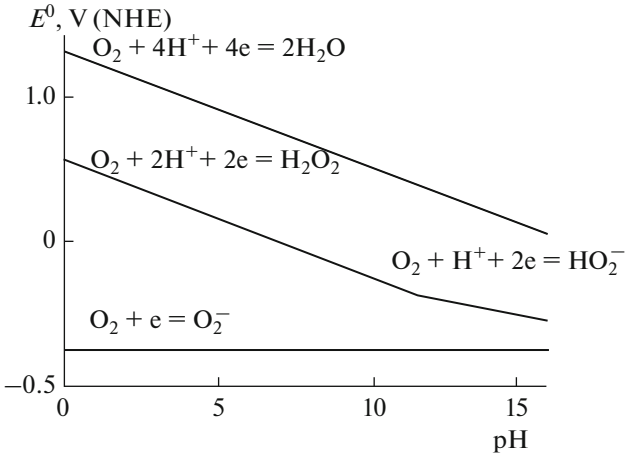

Fig. 1. Diagram $E^0 = f(\text{pH})$ for different oxygen reduction reactions.

2000s and to date, FC of this type are being developed by several small companies in Europe and the USA [4].

The peculiarity of these types of AFC is the use of of liquid or matrix impregnated alkaline electrolytes and the electrodes with the thickness from several tenth fractions to several millimeters and, as a rule, with considerable consumption of noble metals on the cathode, such as PtAu [2] and PtPd [3] alloys, Ag [5]. The works on AFC are partly adjacent to the development of metal-air power sources [6], although the activated carbon-based electrodes cannot be used at high current densities and elevated temperatures.

The use of liquid alkaline electrolytes with sufficient conductivity but large volume failed to stimulate the development of thin electrodes with the thickness within one–two tens of micrometer, in contrast to FC with PEM. Moreover, the use of liquid electrolytes requires special measures on formation of the required ratio of liquid and gas pores [7]. Another drawback of AFC is the electrolyte carbonation, which makes impossible the use of air as oxidant and hydrogen fuel with impurities of CO_2, the product of organic-fuel transformations. The advantage of AFC is the possibility of using hydrogen synthesized by ammonia cracking, as in alkaline media, the ammonia traces do not poison the catalyst, in contrast to FC with PEM.

On the other hand, in the alkaline electrolyte, the potential barrier of oxygen reaction is decreases as compared to PEM with pH value of ~0.2. This is associated with peculiarities of the kinetics and thermodynamics of oxygen reaction (Fig. 1) [8]. The slow stage of O_2 reduction (transfer of the first electron to the adsorbed O_2 molecule) is pH-independent, whereas the equilibrium potential of two- and four-electron mechanisms of O_2 reduction shifts with the pH to the negative direction and in the alkaline region, approaches the potential of the first-electron transfer. In acidic solutions, this difference is compensated by the adsorption energy of the O_2 molecule and its protonation. In alkaline solutions, conditions are created for the materials with relatively low oxygen adsorption energy to become sufficiently active electrocatalysts of its elecroreduction. This extends the range of possible catalytic systems with account taken also of the low corrosivity of alkaline electrolytes. These potentialities of the development of new highly dispersed materials containing no noble metals for AFC with liquid electrolyte were not realized so far.

The further prospects in elaborating this direction are associated with the development and use of anion-conducting polymer electrolytes (ACPE) [9–12]. The relatively low conductivity of these electrolytes requires the development of thin (less than 20–30 μm) electrodes based on catalytic systems with the high conductivity and also with the acceptable mass and volume activities. It is also assumed that ACPE may provide certain other advantages as compared with liquid alkalies. The low solubility of CO_2 in the polymer electrolyte may allow using air as oxidant without special scrubbing; the permissible level of CO and CO_2 impurities in hydrogen fuel increases; the corrosion rate of FC materials in contact with ACPE is lower.

The present study is aimed at generalization and analysis of the state-of-the-art in the field of developing and studying noble-metal-free cathodic catalysts as regards their electrocatalytic activity and selectivity in the oxygen reaction and also their corrosion stability under the conditions of AFC operation. This discussion is based on already published data (predominantly, in the past 5 years) and the results of our own studies.

2. THE MAJOR TYPES OF MATERIALS USED AS CATHODIC NONPLATINUM CATALYSTS AND THE METHODS OF THEIR SYNTHESIS

The list of materials studied with the aim of developing nonplatinum electrocatalysts for various processes of electrochemical power production is constantly extended. The present review discusses the materials showing promise in the development of cathodic catalytic systems for fuel cells with ACPE. These are the highly dispersed carbon materials of different origin [13–15], various types of carbon materials (**CM**) doped with nitrogen [16, 17], boron, sulfur, phosphorus, and transition metals [18, 19], and also complex oxides with the spinel or pervskite structure [20, 21].

The methods of synthesizing highly dispersed CM that can serve both as catalysts and as supports were repeatedly described in the literature and, as a rule, had no direct relation to optimization of catalysts for oxygen reduction; their number constantly increases [22–24]. The oxide, carbide, and nitride systems, especially those with the high chemical and electro-

chemical stability and sufficient conductivity can also serve as the supports [25–27].

Catalytically active materials specially developed for electrocatalysis of the oxygen reaction are synthesized by two principally different methods. The first, more popular method is based on modifying carbon or other supports by different types of precursors including nitrogen and metals, which may be followed by pyrolysis. The literature contains many versions of this method: from simple coadsorption of precursors to carrying out the synthesis in vapors [28] or in plasma [29]. However, irrespective of the synthetic method, the synthesis by the first method retains the support catalytically inert but with the doped surface exhibiting the pronounced catalytic activity. The second method consists in the targeted synthesis of the intrinsically new catalytically active carbon-like material [30, 31] modified with the atoms (N, Co, Fe, etc.) that can enter into composition of the presumed active centers (AC). The introduction of required precursors into some carbon [30] or ion-exchange [32] material is followed by the pyrolysis and the deep activation of the system in ammonia atmosphere until it loses 60–80% of its mass. This method makes it possible to synthesize catalytic systems with the high volumetric concentration of AC.

2.1. Carbon Materials

Highly dispersed CM, namely, activated carbons, carbon blacks, nanotubes, few-layer graphenes, in the absence of additional components exhibit low activity in the cathodic oxygen reduction in acidic electrolytes but display considerable catalytic properties in alkaline electrolytes [14, 15]. In developing nonplatinum catalytic systems, the carbon materials serve not only as the supports but also as the intrinsic catalytic components [33]. The characteristics of carbon supports for cathodic nonplatinum catalysts should meet the following requirements:

—commercial availability and low cost;

—high reproducibility of morphological, structural, and other physicochemical characteristics;

—nanostructuring providing their conjugation with polymer electrolyte molecules;

—high conductivity comparable with metal conductivity;

—chemical and electrochemical activity.

The support function corresponds to those synthetic conditions and methods where the AC formation by modification of the original CM does not induce the changes in CM morphology and structure such that would allow its identification as a new CM. On the other hand, the methods of synthesizing nonplatinum catalysts aimed at production of new CM with the high AC content are being progressively developed [34–36].

Activated carbons (AcC) and carbon blacks formed by turbostratic carbon (TC) are traditionally used for synthesizing nonplatinum cathodic catalysts [13, 14, 23]. The yet newer materials are nanotubes (NT) [37], nanowires (NW) [24], and graphene-like materials, the so-called few-layer graphenes (FG) [38–41].

According to modern views [42], the structural characteristics of highly dispersed CM are determined by the surface and the height of microcrystals forming the carbon material (Fig. 2). Parameters L_a and L_c of microcrystals characterize the size of their basal and side faces. Parameter L_a can be calculated from the width of (110) and (100) peaks in the X-ray spectrum and parameter L_c is calculated based on the width of (002) peak [43]. The structural elements (basal faces and edges) of carbon materials are inherently heterogeneous (anisotropic), like their chemical and electrochemical activity, which is the fundamental property of carbon materials [17]. The electronic properties of carbon materials are also important and critical, because the density of states of electrons (DSE) affects the rate of electron transfer and the rate constant of the electrochemical reaction [18]. In contrast to metals, the DSE of carbon materials varies widely from diamond in which the conduction zone is absent to nanotubes exhibiting well structured DSE and to disoriented carbon materials with relatively high DSE near the Fermi level [42]. This determines the variation of the electric double layer (EDL) capacitance from <2 μF/cm^2 for the basal plane of highly oriented graphite (HOG) to ~60 μF/cm^2 for the edge plane [44] and to 20–24 μF/cm^2 for single-layer graphene [45]. The latter value of EDL capacitance is associated with the extremely high (1.5×10^4 cm^2/(V s)) [46] mobility of carriers. However, this graphene property has not yet been properly used in electrocatalysis.

The intrinsic electrocatalytic activity of carbon materials listed above depends on the ratio of basal and edge structures and, in the general case, is determined by the surface concentration of structural defects. In the framework of these concepts, the highest catalytic activity should be exhibited by AcC that has the least ordered structure [19]. Activated carbons have the finest crystalline structure so that their surface reaches 2000 m^2/g. Their another feature is the presence of a well-developed system of micropores with the characteristic size of <2 nm. Yet another specific feature of AcC is the presence on their surface of various oxygen-containing groups formed during the synthesis and activation of AcC [22, 23].

Oxygen-containing groups can be classified as acidic, neutral, and alkaline (Fig. 3). They are formed mainly on the edges of graphene sheets. Their presence on the basal planes is associated with structural defects. The binding energy of the electron on the sublevel C1*s* for hydrocarbon (C–C, C–H), hydroxyl/ether (C–O), carbonyl (C=O), and carboxyl (O–C=O) bonds is ~285, ~286, ~288, and ~289 eV,

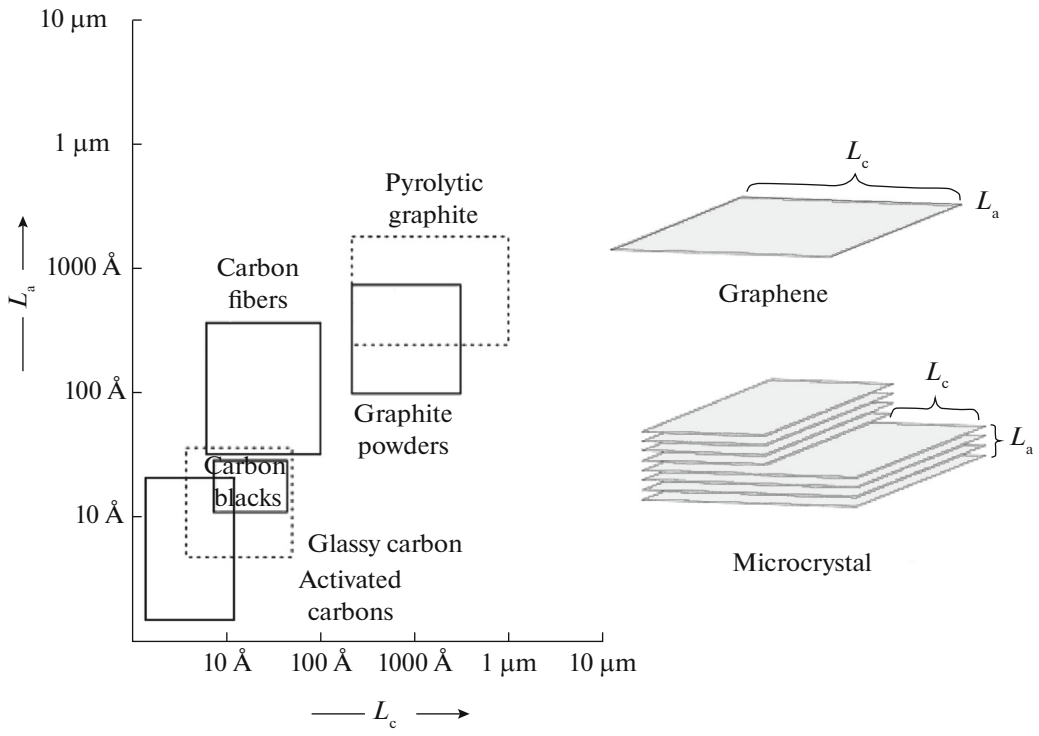

Fig. 2. Approximate grain size of different carbon materials.

respectively [47]. The surface of AcC which has the basic properties acts as the Lewis base and adsorbs protons. The results acquired when studying AcC, are of the general importance for the other allotropic modifications of CM [48]. Besides the oxygen groups formed during the synthesis and determining the surface pH, CM can be modified by "grafted" or adsorbed compounds, such as anthraquinones, phenanthrequinone, naphthoquinones, etc. [49].

Carbon blacks of different origin have the turbostratic structure. Such a structure is based on microcrystal packets representing two-dimensional crystals disoriented along the C axis. The packets are interbound by amorphous carbon of various hybridization. In contrast to AcC, the carbon black particle contains mostly the basal planes on their surface and lacks intrinsic porosity. Table 1 shows certain structural parameters for carbon blacks widely used as the catalyst supports. The presence of microporosity in carbon blacks with the high surface area is associated with the distance between the particles measuring smaller than 10–15 nm.

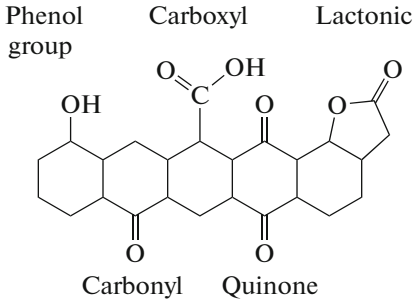

Fig. 3. Oxygen-containing functional groups on the surface of carbon materials.

The low content of the oxidation-prone amorphized carbon and oxidizable structures on the surface of carbon black particles predetermines the higher chemical and electrochemical stability of carbon blacks as compared with AcC. In contrast to the latter, carbon blacks can be graphitized, which increases their corrosion stability but also decreases their specific activity.

Certain advantages over AcC and TC as regards the development of new catalysts are demonstrated by 2D materials: graphenes, graphene-like materials (few-layer graphenes), and also by nanotubes which represent graphene layers rolled into tubes.

—Graphene-like materials and NT contain no disorganized carbon and hence should demonstrate the enhanced chemical and electrochemical stability as compared with AcC and TC.

—FG and NT demonstrate almost the zero forbidden zone, the high mobility of charges, and the high conductivity.

—Active layers based on NT are characterized by high mesoporosity as compared with carbon blacks.

Table 1. Characteristics of commercial carbon blacks [50, 51]

Carbon black	S_{sp}, m^2/g	S_{micro}, m^2/g (V_{micro}, cm^3/g)	S_{meso}, m^2/g	V_{sp}, cm^3/g
Vulcan XC72	227	113 (0.06)	114	0.40
Ketjenblack EC-300	891	482 (0.25)	409	1.02
Ketjenblack EC-600	1405	509	611	2.5
Black Pearl	1567			0.835

—FG and NT are poorly-active catalysts but can be easily modified with atoms of N, B, P, S, I, and also can form composites with complex metal oxides.

—The FG and NT including their chemical modifications can be synthesized in large amounts at low cost.

The synthesis of NT, their cleaning and functionalization before the preparation of catalysts are described in detail [52]. The simplest and cheapest method of synthesizing few-layer (up to 6–7 monolayers) graphene materials is the splitting of graphite oxide (GO) at the chemical, thermal, or electrochemical reduction. As was shown [44], the edges of graphene sheets are intrinsically active as compared with their basal plane. In terms of this general approach to assessing the activity of edge structures as compared with the basal plane, one cannot expect any special electrocatalytic properties for graphene and graphene-like materials that retain the main properties of graphene.

The use of polymer membranes and polymer electrolytes in the composition of active layers requires taking into account the ratio of characteristic sizes of micropores (slot structures) which contain AC localized on graphene-sheet edges and ionomer's polymer chains with sulfo-groups with the size of ~2 nm. The ratio of these geometrical sizes fails to provide the immediate contact between an AC in a micropore and a sulfo-group in a polymer chain. However, the high characteristics attained for microporous nonplatinum catalysts [31, 32] and the theoretical studies [53] have shown that such contact can apparently take place as a result of the extension of the proton field beyond the polymer chain. This places AcC among the promising supports for catalytic systems for polymer electrolyte.

2.2. Carbon Materials Modified with Nitrogen

When considering the catalytic properties of nitrogen-doped carbon materials, two problems are the most important: which methods should be used for synthesizing metal-free carbon materials doped with nitrogen and whether the doping with nitrogen in the absence of transition metals can produce catalysts selective with respect to the direct four-electron oxygen reduction reaction.

Nitrogen-doped carbon materials have become the object of studies relatively recently. Despite being still very few, the number of works devoted to experimental investigation of the catalytic properties of N-doped carbon materials in O_2 reduction increases quite quickly [54–65]. The catalytic properties of metal-free heteroatom-doped graphene materials were surveyed in [66].

In this field, in contrast to carbon materials doped with both nitrogen and metal, at present it is difficult to distinguish any definite tendencies. However, as demonstrated below, the majority of authors associate the catalytic activity of N-doped carbon materials precisely with N-doping, i.e., upon its substitution for carbon atoms, nitrogen incorporates into the structure of the carbon material to produce its pyrrole, pyridine, or graphite forms.

Catalyst-free spray-pyrolysis of the xylol–ethylenediamine mixture at 1000°C on a quartz support yielded N-doped spherical particles containing from 0 to 6.2 wt % of N, with the diameter of 130–500 nm and the specific surface of 11–13 m^2/g [56]. The XRD spectra demonstrated peaks at 25 and 43.8 deg, pertaining to graphite planes (002) and (100), respectively. Their considerable broadening pointed to the low degree of graphitization. According to XPS data, the material contained C, N, and O atoms. Catalyst-free pyrolysis of the mechanical mixture of oxidized graphite synthesized by the Hammers method and melamine at 800°C in the Ar atmosphere produced flat nanosheets with the thickness down to 1 nm and a sufficiently high degree of graphitization [57], which was confirmed by XRD data: the basic plane C1*s* with the binding energy of 284.4–284.8 eV, which is typical for carbon with sp^2 hybridization. The X-ray patterns demonstrated the broadened peaks typical for (002) graphite face at 25.9 deg with the interatomic distance of ~0.35 nm. According to XRD data, the surface-layer composition included atoms of C, N, and O. The nitrogen content could reach 10.1 at %. In [49], a C_3N_4/carbon support composite was synthesized with the ordered structure of interconnected mesopores. The synthesis was carried out by catalyst-free pyrolysis of cyanamide (CH_2N_2) applied by impregration on the

surface of the carbon/SiO_2 composite at 500°C in inert atmosphere. The carbon phase of the composite was obtained by the pyrolysis at 900°C of saccharose on the surface of silicon dioxide. The catalyst porosity formed by etching was determined by the size of etched-out silicon-dioxide particles. Thus, the use of SiO_2 with particles of 12 nm allowed to synthesize a mesoporous composite with the specific surface of 996 m^2/g and the use of SiO_2 powders with the size of 150, 230, and 400 nm produced macroporous composites with the specific surface of 97, 58, and 60 m^2/g, respectively. In [59], the properties of nanocylinders formed by carbonization of polyaniline salts in the N_2 atmosphere at 800°C in the absence of metal catalysts and supports were characterized in detail. These cylinders had the diameter from 35 to 220 nm, the specific surface from 310 to 440 m^2/g and were characterized by the high fraction of micropores (from 62 to 90%) for their specific volume of up to 0.185 cm^3/g. The specific conductivity of nanocylinders was 0.3–0.8 S/cm. They contained a high fraction of amorphous carbon, as follows from the Raman-spectroscopy-acquired ratio $I_D/I_G = 3.48–3.68$. According to XPS data, the nitrogen content reached 7 at %. In [60], the properties of composites of melamine, urea, and dicyanodiamide with a graphene-like material with the mass ratio of 1/20, synthesized by catalyst-free pyrolysis in Ar at 800°C were studied. According to XPS data, the nitrogen content in these composites reached 5 at % for the pyridine form fraction reaching 45 at %. In [17], vertical nanowalls with the thickness from 0.5 to 4.5 μm determined by the deposition time (6–25 min) were grown on the surface of glassy carbon or silicon by a the catalyst-free method that consisted of their plasma-chemical deposition from a $CH_4 : H_2$ mixture at temperatures of 730 and 860°. The original nanowalls were ~20–40 nm wide and ~3–5 nm thick, which corresponds to 9–12 graphene monolayers. The plasma treatment in the N_2 : Ar mixture produced N-doped materials with the nitrogen content from 4 to 20 at %. The total content of nitrogen and the relative content of its forms (pyridine/pyrrole + amine/graphite + quaternary/oxidized) depended on the temperature and the power (200–600 W) of plasma treatment.

The group of N-doped systems containing no metal atoms also includes various NT [67] and nanofibers (**NF**) after subjecting them to thorough removal of traces of metals-catalysts (Ni, Fe, Co) involved in formation of the specific structure of these carbon materials. In [68], the synthesis of vertical NT by decomposition of Fe(II) phthalocyanine followed by complete removal of Fe by the electrochemical treatment was described. The authors assumed that the activity of these NT with the length of 8 μm and the diameter of 25 nm exceeded the platinum activity due to their N-doping. However, it deserves mention that the possibility of synthesizing N-doped NT totally free of metals is called into question and the catalytic effects of such materials can often be explained by the presence of transition metal traces [69].

2.3. Carbon Materials Modified with both Nitrogen and Transition Metals

This group of materials includes, as a rule, the products of thermal treatment of nitrogen containing organic compounds, obtained in the presence of iron-group transition metals. The thermal treatment is carried out at 700–900°C in inert atmosphere. The time of thermal treatment amounts, as a rule, to 1–2 h. On the other hand, low-temperature synthetic methods were also used [70]. The best-studied nitrogen-containing precursors for the synthesis of nitrogen-modified carbon materials include N_4-complexes, i.e., metal phthalocyanines and metalloporphyrins (most often, TMPPCo and TMPPFeCl) [18]. However, the high cost of N_4-complexes and the low yield of pyrolysis products limit their use in the large-scale synthesis of catalysts. For instance, the yield of TMPPCo pyrolysis product adsorbed on Vulcan XC72 in the amount of 30%, was less than 40% at 850°C [71]. As the nitrogen-containing precursors, the simpler organic complexes were also used, such as complexes of phenanthroline [72] and ethylenediamine [73] and also polymers such as polyacrylonitrile (PAN) [74], polyaniline (PANI) [75], polypyrrole (PP) [76], etc. As the gaseous sources of nitrogen at plasma treatment, ammonia [77, 78] and N_2 were utilized [79]. Thus, the activation in the NH_3 atmosphere made it possible to increase the specific activity of pyrolysis products of metalloporphyrins [77] considered so far as the most active catalysts of O_2 reduction among the N-doped carbon materials in both acidic and alkaline media. The catalysts were synthesized by pyrolysis of both supported precursors and those without supports. The supports used most often were carbon materials (carbon blacks of various degrees of dispersion, graphite powders, powders of graphene-like materials, nanotubes) and oxides (Al_2O_3, SiO_2). The oxides pertain as a rule to the removable supports, which allows the catalyst with high porosity and well-developed surface to be synthesized [80]. The pyrolysis of nitrogen-containing precursors in the absence of special pore-forming agents (e.g., oxalates in [35]) or involving no special forming procedures (as for PAN fibers in [81]) leads to sintering of the precursor to yield a coarse powder with low catalytic activity.

The method used most actively for synthesizing catalysts includes the following sequence of operations: adsorption of the nitrogen-containing precursor and metal-containing compounds on the support surface → pyrolysis → washing.

It was shown experimentally that to synthesize active catalysts selective with respect to the four-electron oxygen reduction reaction, the pyrolysis should be carried out in the simultaneous presence of carbon, nitrogen, and transition metals atoms [19]. Separate pyrolysis of supported metal compounds or metal-free nitrogen compounds gives no way of synthesizing efficient catalysts. The role of each component mentioned above was discussed in [82] and will be briefly discussed in Section 5.1 "Active centers of carbon materials modified with nitrogen and transition metals."

According to the results of elemental analysis, the main components of catalysts are carbon, nitrogen, and metal. The carbon content can reach 90–95%. Carbon can be involved in the catalyst composition as the catalytically-inert carbon support and also as the pyrolysis product as such which is a semiconductor. According to XPS data, carbon can be present in the sp^3- (C1s E_b = 285 eV) and sp^2- (E_b = 284.4 eV) hybrid states, in its oxidized state in the form of oxygen-containing groups (E_b = 286–289 eV), and in composition of metal carbides. The effect of the ratio of different carbon forms on the catalytic activity of materials was not studied so far. However, according to modern views, the most probable localization of the catalytically active centers of O_2 reduction are the faces of graphite crystals [83–85], i.e., the catalytic properties are determined by the relative intensity of the sp^2-hybride state of carbon in the pyrolysis product as such. The nitrogen content is low (up to 2%), which is due to the high pyrolysis temperature, and includes pyrrole (N1s E_b = 400.2–400.9 eV), pyridine (E_b = 397.0–399.5 eV), graphite (E_b = 401–403 eV), and oxidized (E_b = 402–405 eV) nitrogen [36]. It was shown [86] that the catalyst is stable if pyridine nitrogen undergoes no chemical transformations. The graphite form is the most stable form of nitrogen in the structure of carbon materials [47]. It was shown that the metal amount higher than ~2% not only exerts no positive effect on the catalytic properties but even decreases the latter [87]. To confirm the fact that metal particles were not the active centers on carbon materials doped with nitrogen and transition metals, the catalyst was washed in concentrated acid solution (e.g., 12 M HCl) at temperatures up to 80°C to decrease the metal content down to several ppm [88]. In several studies, it was demonstrated that elemental sulfur is a useful additive that binds the excessive iron during pyrolysis thus preventing the formation of iron nitrides and carbides but leaves untouched nitrogen and carbon which are the potential active-center components [89]. The surface composition may also include up to 5% of oxygen within functional groups.

Measuring CV of the pyrolysis products of TMPPFeCl in 1 M NaOH has shown that the thermal treatment at temperatures above 400°C results in destruction of metalloporphyrin molecules and the destruction process is completed in the temperature range of 500–600°C. This was indicated by the total disappearance of the anodic and cathodic CV peaks at 0.3 and 0.25 V, respectively, which are typical for the reaction Fe(III) + e ↔ Fe(II) [90]. In [91], using the Mössbauer spectroscopy, it was shown that pyrolysis at 850°C of 4.8% TMPPCo adsorbed on Vulcan XC72 carbon black resulted in the break of Co–N bonds to form metal oxides.

2.4. Complex Oxides

Oxide catalytic systems always attracted attention as the possible cathodic catalysts for AFC. Thus, the first sufficiently powerful AFC employed lithiated nickel oxide [92]. Among simple oxides, attention was focused on CoO_x [93] and MnO_x [94]. These oxides were used both as individual catalysts and for additional doping of pyropolymers of N_4-complexes [95] with the aim of accelerating the decomposition of HO_2^-, the product of incomplete reduction of oxygen. Furthermore, the stability of simple oxides in concentrated alkaline solutions at 60–90°C is not sufficient for their successful use in AFC.

The $MgAl_2O_4$ spinel structure is typical for complex oxides $A^{2+}B_2^{3+}O_4$ (its more general composition is $A_x^{2+}B_{3-x}^{3+}O_4$, where $0 < x \leqslant 1$). In normal spinels, cation A is bivalent (Mg^{2+}, Mn^{2+}, Fe^{2+}, Ni^{2+}, Zn^{2+}, Co^{2+}), and cation B is trivalent (Al^{3+}, V^{3+}, Cr^{3+}, Fe^{3+}, Mn^{3+}, Co^{3+}). The spinel crystal has face-centered cubic lattice with oxygen atoms in its lattice sites. The interstices are partially occupied by cations. The spinel unit cell includes 8 cations A, 16 cations B, and 32 oxygen atoms. For 32 oxygen atoms in the closest packing, there are 32 octahedral and 64 tetrahedral voids of which 8 tetrahedral (A sites) and 16 octahedral (B sites) voids are occupied by cations [96]. In formulas of normal $A[B_2]O_4$ and inverse $A[AB]O_4$ spinels, the cations that occupy B sites are taken in brackets. The size of cations in B sites (octahedral voids) is as a rule higher as compared with cations in A sites (tetrahedral voids). Figure 4 illustrates the spinel structure.

In compounds with the $CaTiO_3$ perovskite structure and isomorphous compounds with the general composition $A^{m+}B^{n+}O_3$ (where m/n = 1+/5+; 2+/4+; 3+/3+) and the primitive cubic lattice, the larger cations A are localized in the cell center, the smaller cations B occupy the cube vertices, and oxygen ions are in the middle of edges [97], as shown in Fig. 5.

The traditional methods for synthesizing complex oxides are the direct thermal decomposition of salt melts and codeposition of salts (hydroxides, oxalates) followed by thermal decomposition [98] and pyrolysis [99]. These methods require elevated temperatures for overcoming the diffusion barrier in the synthesis of complex oxides and give no way of producing highly dispersed materials. In [100], using the method of

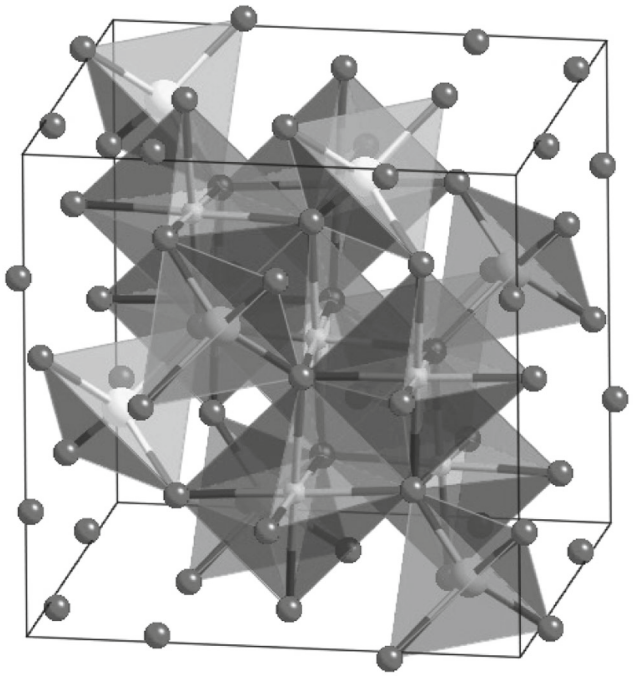

Fig. 4. Crystal structure of spinel $A[B_2]O_4$.

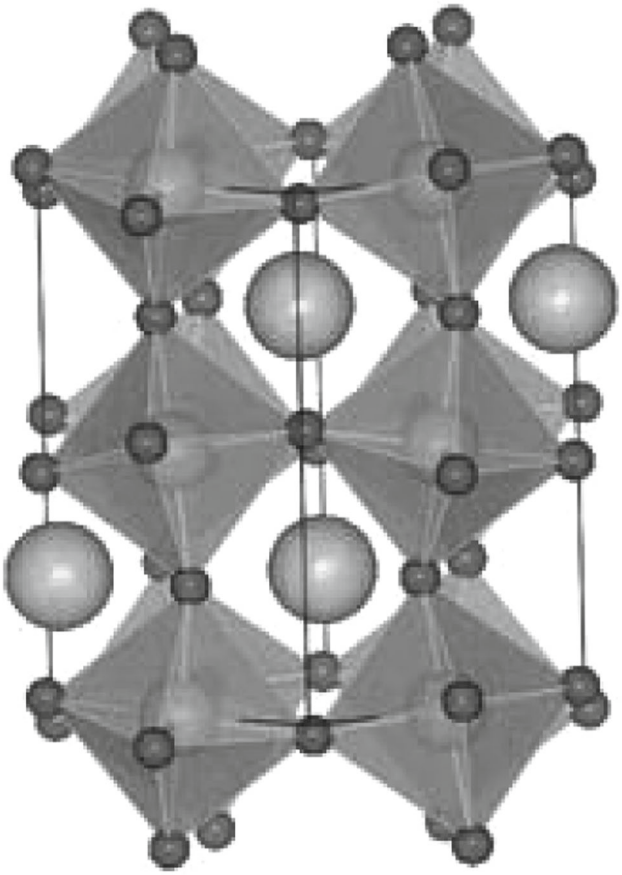

Fig. 5. Crystal structure of perovskite.

codeposition in the presence of alcohols that prevents the crystal growth, a series of catalytic systems $LaMnO_3$/Ketjenblack EC-600 with the perovkite content from 10 to 100 wt % were synthesized. The crystal size varied from 17 to 28 nm, respectively.

For synthesizing oxide catalysts, cryochemical methods were also used, namely, sublimation drying and crystallization by freezing [99]. Recently, the sol–gel method [101], a method of codeposition at low temperature [102, 103], and the inverse micelle procedure [104, 105] were introduced into practice. These methods allow catalytic systems with the high specific surface to be synthesized, which is necessary for their use together with polymer anion-conducting electrolytes. For instance, the $La_{0.4}Ca_{0.6}Mn_{0.9}Fe_{0.1}O_3$/Ketjen Black EC-600 catalyst with the average size of particles of 2.5 nm was synthesized by the method of inverse micelles [105].

3. THE MAIN APPROACHES TO ASSESSING ACTIVITY AND SELECTIVITY OF SYSTEMS CONTAINING NO NOBLE METALS

The correct determination of the catalytic activity of highly dispersed catalytically active materials requires measuring the kinetic parameters undistorted by transport limitations. At present, the majority of model studies of kinetic characteristics of O_2-reduction catalysts of different degrees of dispersion (with the particle size from several nanometers to several micrometers) are carried out by the method of rotating disk electrode (RDE).

The RDE method is based on the equal diffusion accessibility of the electrode surface at forced agitation. The method is described by Eqs. (1)–(3) [106].

$$\delta_{dif} = 1.61 D^{1/3} \nu^{1/6} \omega^{-1/2}, \quad (1)$$

$$I_{dif}^{lim} = 0.62 n F c_{O_2} D^{2/3} \nu^{-1/6} \omega^{1/2} \quad \text{(Levich equation)}. \quad (2)$$

According to Eq. (2), the slope of the linear dependence I_{dif}^{lim} vs. $\omega^{1/2}$ allows the number of electrons n trasfered to O_2 to be determined. According to Eq. (3) proposed by Frumkin [107] and widely known as the equation of Koutecky–Levich [108], the linear dependence $\frac{1}{I_{exp}}$ vs. $\omega^{-1/2}$ makes it possible to determine the kinetic current I_{kin} and n.

$$\frac{1}{I_{exp}} = \frac{1}{I_{kin}} + \frac{1}{I_{dif}^{lim}} = \frac{1}{knFSc_{O_2}} + \frac{1}{I_{dif}^{lim}}. \quad (3)$$

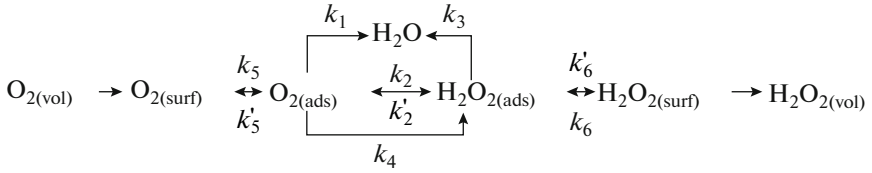

Fig. 6. Scheme of the parallel-sequential reaction of O_2 electroreduction.

As was noted in [106], the use of Eq. (3) for calculating n is possible only for simple two- (k_2) or four-electron (k_4) processes, or for the reaction of O_2 reduction proceeding by the parallel path to yield H_2O (k_1) and H_2O_2 (k_2), when the constants k_3 and k_4 are negligible, as observed, e.g., for catalysts TMPPCo/Vulcan XC72 [109], PdCo/TMPPCo/C [110], and Mn–Co spinels [111]. In the latter case, the quantity n determined based on Eq. (3) corresponds to a certain average value. For catalysts on which the O_2 reduction proceeds by the parallel-sequential path, e.g., for TMPPFeCl/Vulcan XC72 (see below), Pt [112], or Mn–Co spinels [113], the equation of Koutecky–Levich cannot be used.

At present, the only well-substantiated method of assessing the catalyst selectivity with respect to O_2 reduction is the method of rotating ring-disk electrode (RRDE), the theory and applications of which are described in details in [106]. Figure 6 shows the simplified scheme of O_2 reduction used in the analysis by the RRDE method. Equations (5) and (6) [106] are used for calculating the rate constants.

$$\frac{I_D N}{I_R} = 1 + 2\frac{k_1}{k_2} + \frac{k_3 + (k_3 + k_4)\left(1 + 2\dfrac{k_1}{k_2}\right)}{0.62 D_{H_2O_2}^{2/3} \nu^{-1/6}} \omega^{-1/2}, \quad (4)$$

$$\frac{(I_{dif}^{lim} - I_D)N}{I_R} = 1 + 2\left(\frac{D_{O_2}}{D_{H_2O_2}}\right)^{2/3} \times \frac{k_3 + k_4}{k_2} + 2\frac{0.62 D_{O_2}^{2/3} \nu^{-1/6}}{k_2} \omega^{1/2}. \quad (5)$$

In the recent studies of nonplatinum catalysts of O_2 reduction, the gradual transition was observed from the thin-layer RDE method, the closest to the authentic RDE method destined for studying smooth surfaces, to the "thick-layer" version used for real electrodes [114]. The layer thickness can reach several tens of micrometer for loadings of up to 1–2 mg per cm^2 of the geometric surface.

To characterize the catalytic activity and selectivity of CM of different origin and also of oxide materials with respect to O_2 reduction, it is recommended to carry out measurements both by means of thin-layer version of RDE and RRDE methods (with the layer thickness of 1–2 μm) and by studying the effect of the layer thickness on certain parameters. These parameters include the overall current (i_{exp}); onset potential (E_{on}); the half-wave potential ($E_{1/2}$); the specific mass activity (i_{mas}); the specific activity per unit of real surface (i_{sp}); the limiting diffusion current (i_{lim}); the collection efficiency (N); the Tafel slopes (b); the interval of loading m within which the specific mass activity is independent of the amount of loaded material.

In ref. [71] devoted to studying the effect of loading m in the interval of 0.02–1.00 mg/cm^2 (or in the thickness L interval of 0.5–26.3 μm) on the accessibility and selectivity of 30% TMPPCo/Vulcan XC72 catalyst in 0.5 M H_2SO_4 at 60°C, the parameters were determined: b, n, i_{sp}, E_{in}, $E_{1/2}$, and the yield of hydrogen peroxide. By RDE and CV methods, the effect of the layer thickness of Vulcan XC72 and TMPPCo/Vulcan XC72 composite on the specific mass activity i_{mas} and the specific charge Q_{mas} was studied [109, 115]. Figure 7 shows that for $m < 1$ mg/cm^2, the Q_{mas} value for Vulcan XC72 was constant and i_m decreased even for $m > 0.1$–0.2 mg/cm^2. This is why a layer of Vulcan XC72 in an alkaline electrolyte was equally accessible only for m below 0.1–0.2 mg/cm^2 ($L < 5$ μm). In alkaline electrolyte, the upper limit of L ensuring the catalyst equal accessibility for O_2 molecules does not exceed ~5 μm, as for carbon blacks (Fig. 8).

For catalytic materials synthesized by pyrolysis of nitrogen-containing compounds applied on carbon supports, the modern methods give no way of differentiating between the intrinsic specific surface of the pyrolysis product and the initial carbon support. The specific mass activity is a more universal characteristic; however, it can be used only for comparing materials of the same nature. The specific volumetric activity, i.e., the activity per volume unit of the catalyst layer, which includes the value of the specific mass activity and takes into account the geometrical parameters of the real electrode, makes it possible to assess the catalyst efficiency as a function of its layer thickness. This is why the value of volumetric activity proposed in [116] is apparently the convenient parameter for comparing the activities of various electrode materials regardless of their nature.

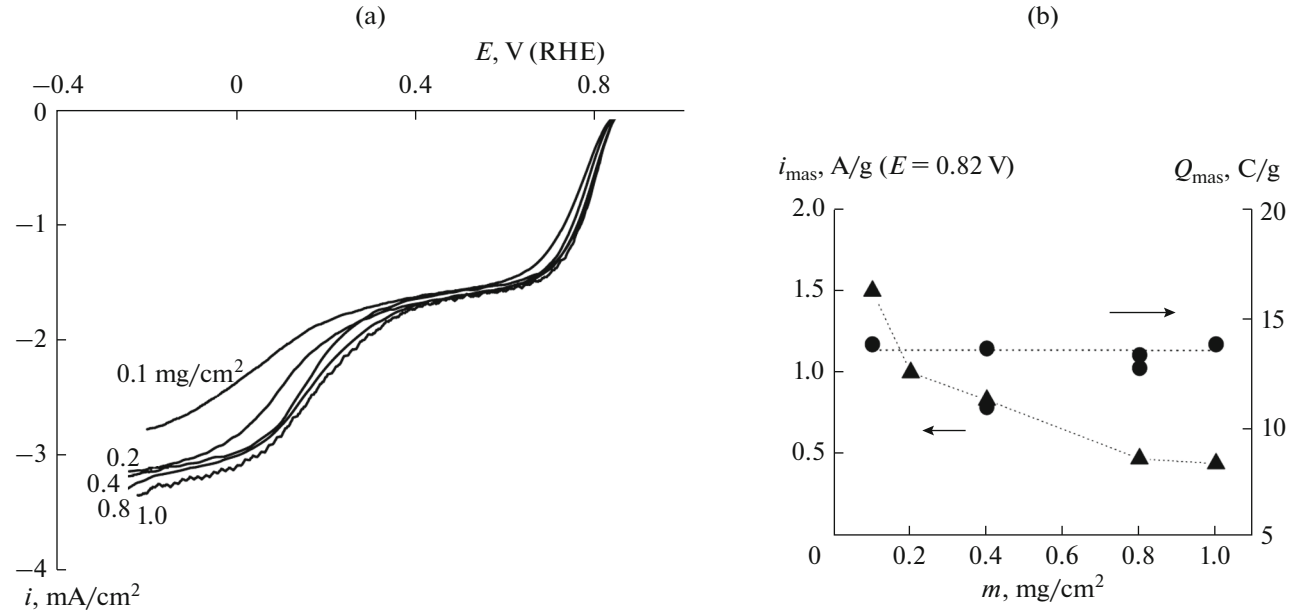

Fig. 7. (a) Polarization curves of O_2 reduction on Vulcan XC72 measured at m variation RDE, 1 M KOH, O_2, 60°C, v = 1 mV/s, ω = 1580 rpm. (b) Dependence of the specific mass activity i_{mas} and the specific charge Q_{mas} on the catalyst loading.

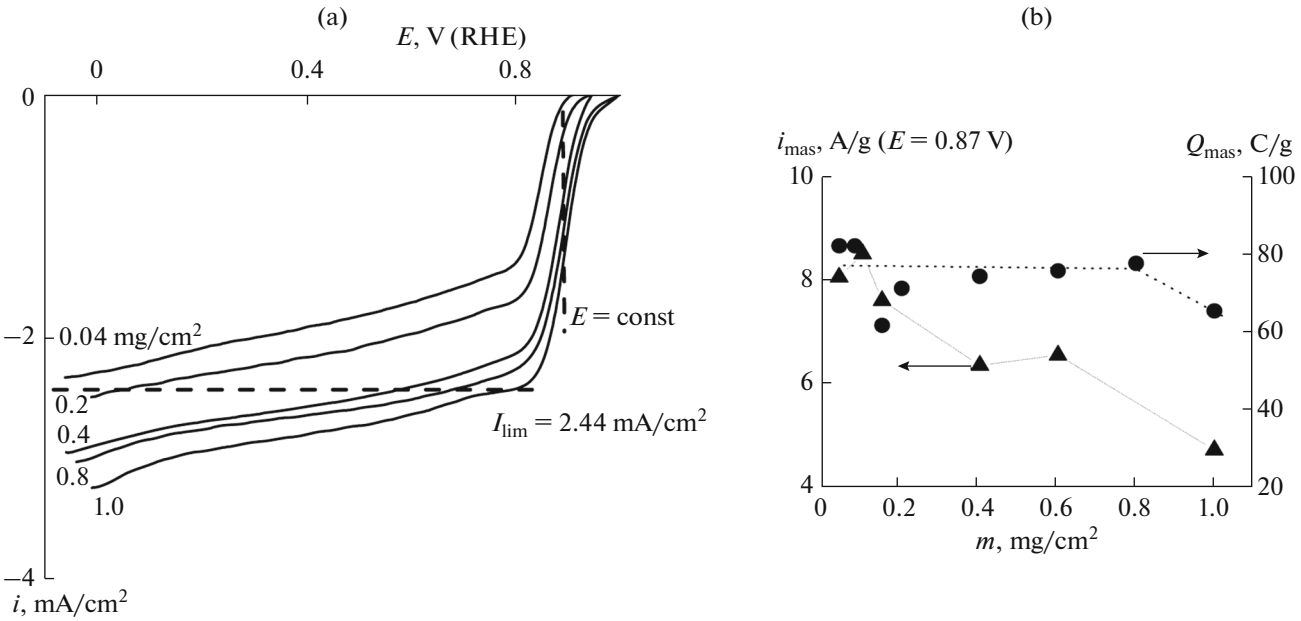

Fig. 8. (a) Polarization curves of O_2 reduction on 30% TMPPCo/Vulcan XC72 catalyst measured at varying m RDE, 1 M KOH, O_2, 60°C, v = 1 mV/s, ω = 1580 rpm. (b) Dependence of the specific mass activity i_{mas} and the specific charge Q_{mas} on the catalyst loading.

4. COMPARATIVE KINETIC CHARACTERISTICS AND SELECTIVITY OF PROMISING CATALYSTS UNDER MODEL CONDITIONS

4.1. Carbon Materials Doped with Nitrogen

As noted above, both catalyst-free and catalytic methods can be used for synthesizing N-doped carbon materials.

It was shown [56] that in 0.1 M KOH, the onset potential values of O_2 reduction on 20% Pt/C and the composite synthesized by catalyst-free pyrolysis of the xylol/ethylenediamine mixture in the amount of ~300 μg/cm^2 were close to one another being equal to ca. –0.1 V (Ag/AgCl), and the slope found according to the Koutecky–Levich equation at the potential of –0.35 V (Ag/AgCl) corresponded to 3.86 electrons per oxygen

molecule. However, these polarization curves exhibited two successive waves. The first-wave height corresponds to the limiting diffusion current of the two-electron process. The potential of –0.35 V (Ag/AgCl) falls in the region of this wave and corresponds to O_2 reduction to HO_2^- and to the number of electrons 2 rather than the number 3.86 shown by the authors. The polarization curves on Pt catalyst was also assumed to comprise two waves, which contradicts the numerous available experimental data pointing to the single-wave polarization curve on Pt [117].

According to the results obtained by means of RRDE method in 0.1 M KOH [57], the polarization curve of O_2 reduction on the catalytic systems synthesized by catalyst-free pyrolysis of oxidized graphite and melamine shifts by 0.1 V in the positive direction as compared with the unmodified GM. O_2 reduction is characterized by a single wave and the number of electrons amounts to 3.4–3.6 in contrast to 2.2–2.4 for unmodified CM.

Measuring polarization curves by means of RDE in 0.1 M KOH has shown [58] that O_2 reduction on C_3N_4/carbon support composites prepared by etching out SiO_2 supports of different degrees of dispersion is characterized by a single wave. The specific surface of composites insignificantly affected their activity and the number of electrons (n = 2.9–3.2) calculated based on Eq. (3).

According to the results obtained by RDE method in 0.1 M KOH [59], for the catalyst loading of 250 μg/cm^2, onset potential of O_2 reduction on the pyrolysis products of PANI nanocylinders was ~–0.2 V (Hg/Hg_2Cl_2). Depending on nitrogen content and the specific surface value, the number of electrons determined using Koutecky–Levich equation decreased in the series 7.04 at % (including 3.61 at % of pyridine N, the total specific surface 317 m^2/g) > 5.83 at % (2.04 at %, 322 m^2/g) > 5.5 at % (2.25 at %, 441 m^2/g), being equal to 3.5 > 2.5 > 1.8, respectively. As the catalyst amount increased from 250 to 500 μg/cm^2, the average number of electrons involved in the reaction was found to increase. The authors observed also a correlation between the specific mass activity and the specific surface of mesopores. Unfortunately, the specific catalytic activity and the number of electrons were determined at the potential of –0.6 V (Hg/Hg_2Cl_2) where the limiting diffusion current was already attained. Moreover, the polarization curves were measured with a relatively high potential scan rate of 20 mV/s, which means that the contribution of charging currents to the recorded current may be high. This followed from cyclic voltammograms also recorded at the rate of 20 mV/s. Probably, this was due to some methodical error giving rise to a correlation between the catalytic activity and the capacitance value, revealed by the authors.

When studying the properties of composites formed by melamine, urea, and dicyanodiamide with a graphene-like material, which were synthesized by uncatalyzed pyrolysis, the authors of [60] stated that the number of electrons determined using Eq. (3) for unmodified graphene-like materials was 2 at potentials more positive than –0.8 V (Hg/Hg_2Cl_2) and 2.8 for the more negative potentials in the second-wave region. For the melamine-based composite, the number of electrons increased under the same conditions from 2.5 to 3; for the urea-based system, it increased from 3 to 3.8, and for dicyanodiamide, from 3.5 to 4. However, according to the character of polarization curves measured by RDE method on the initial graphene-like material and also on its composites based on melamine and urea, the reaction of O_2 reduction in 0.1 M KOH proceeded only by the sequential path through the formation of hydrogen peroxide. This followed from the presence of two clearly pronounced waves.

The CV studies of undoped and N-doped nanowalls in 0.1 M KOH [17] made it possible to relate the increase in capacitance to the increase in the layer thickness and also to degree of N-doping. The doping shifted onset potential by 60 mV in the positive direction. The shape of polarization curves and the values of limiting diffusion current close to their value calculated for n = 2 suggest that the reaction of O_2 reduction proceeds by the successive route both on doped and undoped materials. According to the authors, at 0.38 V (RHE) (in the second-wave region), n = 2.1–4, which, however, does not imply direct four-electron process.

The catalytic activity and selectivity in 0.1 M KOH of metal-free N-doped carbon aerogels synthesized by the high-temperature treatment (700–900°C) of preliminarily carbonized nanofibers of bacterial cellulose in NH_3, were compared with the literature data and also with the results for ammoxidized carbon blacks Vulcan XC72, Ketjenblack EC-300, carbon nanotubes, and reduced graphene oxide [118]. By means of RRDE method, the average number of electrons for nitrogenized carbon blacks at 0.8 V was found to not exceed 2.5, whereas for N-doped aerogels based on carbonized cellulose and graphene oxide, this number amounts to 3.96.

According to ref. [82], on nitrogen-doped CM, O_2 reduction in alkaline electrolytes proceeded by the sequential path, the same as on unmodified CM. Figure 9 shows polarization curves of O_2 reduction on carbon black Ketjenblack EC-300; carbon black Ketjenblack EC-300 modified with 40 wt % PAN pyrolyzed at 900°C; dispersed electrospun mat PAN-900 pyrolyzed at 900°C; and PAN-6 fibers activated in water vapors at 1000°C. According to XPS data, PAN-900 contained up to 10 at % nitrogen for its specific BET surface not exceeding 100 m^2/g. According to the BET data, PAN-6 had the specific surface of up

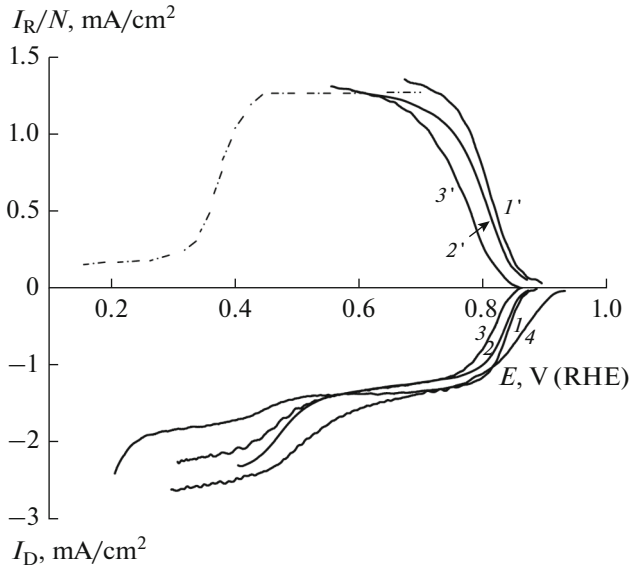

Fig. 9. Polarization curves of O_2 reduction of a disk electrode (I_D) and the currents of H_2O_2 oxidation on Pt ring (I_R) for (*1*, *1'*) 40% PAN-900/Ketjenblack EC-300; (*2*, *2'*) Ketjenblack EC-600; (*3*, *3'*) PAN-900; (*4*) PAN-6. RRDE, 1 M KOH, O_2, 1 mV/s, 25°C, 660 rpm, loading 200 μg/cm^2.

to 1600 m^2/g, the adsorption capacity with respect to benzene vapor of 570 mg/g, and the nitrogen content found by elemental analysis of 2.7 wt %.

A series of studies [119, 120] were devoted to the effect of nitrogen atoms on the properties of nanowires in O_2 reduction reaction. The materials were synthesized by deposition of vapors of ferrocene and *m*-xylol or pyridine. It was shown that the rates of O_2 reduction and H_2O_2 decomposition were accelerated with the increase in the degree of N-doping, being independent of the presence of Fe. This is why, presumably, Fe played the role of the catalyst in the stage of synthesis.

The effect of nitrogen content (melamine served as its source) in NT synthesized at 800–1000°C in presence of ferrocene as the catalyst was studied in O_2 reduction reaction in 0.1 M KOH [121]. As the nitrogen content increased from 0 to 7.7 at %, the E_{st} value increased from 0.767 to 0.947 V (RHE). For nitrogen amount higher than 3%, a single polarization wave was observed and, according to Koutecky–Levich equation, $n \sim 3.7$. Polarization curves of O_2 reduction were measured for the catalyst loading varying from 20 to 800 μg/cm^2. The highest mass activity at $E = -0.15$ V (RHE) attained for the catalyst loading of 160 μg/cm^2 was comparable with the characteristics of the electrode containing ~2 μg/cm^2 Pt.

In other ref. [122] carried out on NT, doped with nitrogen during their synthesis in presence of ferrocene as the catalyst, followed by Fe removal, the polarization curves were shown to have two waves. Although the number of electrons calculated based on Koutecky–Levich equation was 3.6–3.8, four-electron reaction cannot be assumed in view of aforesaid. It was suggested that the role of the metal consisted in catalyzing the reaction of nitrogen incorporation into the NT structure [16, 123].

Based on the analysis of different mechanisms of O_2 reduction on Pt/C catalyst and nitrogen-doped NT carried out by polarization curves fitting, it was shown that in the both catalytic systems the reactions proceed by close pathways in alkaline electrolyte [124]. For the direct reaction, the rate constants k_1 exceeded k_2. Moreover, the rate constant for the reduction of perhydroxyl ion k_3 was quite considerable which led to the apparent four-electron path.

Highly efficient catalysts based on ethylenediamine and salts of Fe and Co in the 1/1 metal ratio were described [125, 126]. Their synthesis was carried out at 900°C in inert atmosphere. The subsequent treatment in 0.5 M H_2SO_4 followed by repeated thermal treatment at 900°C resulted in disappearance of the peak in *i* vs. *E* curves in 0.1 M KOH near 0.1–0.2 V (RHE) associated with the presence of metal. The Tafel slope was ~–0.07 V/decade. The half-wave potential was 0.1 V more positive as compared with the original carbon material and 0.025 V more cathodic as compared with the platinum system 46 Pt/C (TKK).

The characteristics of a catalyst synthesized on SiO_2 with the use of polyethyleneimine as the source of nitrogen and carbon in the presence of salts of Co, Fe, Ce, which was followed by the removal of SiO_2 and virtually all metals by treatment in HF, were described [127]. The Co-containing system exhibited the highest activity.

The results found for platinum-free systems with sufficiently well removed metals differed insignificantly from the data for nitrogen-containing CM derived without using metal catalysts. More diverse experimental data characterizing the dependence of the kinetics of O_2 reduction and its selectivity on the nature of metals were acquired for CM simultaneously doped with nitrogen and a transition metal.

4.2. Catalysts Containing Nitrogen and Transition Metals

As compared with the other groups of carbon-supported nonplatinum catalysts, the systems containing nitrogen and transition metals exhibit the higher activity and the higher selectivity with respect to four-electron reaction and demonstrate a pronounced effect of metal atoms on the catalytic properties. In this group of studies, attention was focused on the use of graphene-like materials as the supports. This is associated with the high surface of graphene (theoretical value ~2630 m^2/g), its adequate chemical stability, high conductivity, unique structure of the graphite basal plane including its susceptibility to functional-

ization. Among various heteroatoms (N, B, P, S), nitrogen is highly advantageous as regards modifying graphene-like materials due to the close atomic sizes of nitrogen and carbon and the possibility of forming a strong covalent bond with carbon atoms. The theoretical investigations [128] have shown that nitrogen can be considered as the *n*-donor that transfers electrons to carbon favoring the formation of disoriented carbon. The studies by adsorption spectroscopy [129] have shown that the defects in the carbon structure can bind nitrogen and then coordinate Fe or Co. As compared with the other types of CM, graphenes have the largest number of active sites for binding N and coordinating metals [130].

Catalysts with the high activity in alkaline electrolytes were synthesized [131] based on oxidized graphene, as the main component, ethylenediamine, melamine, and PANI, as the nitrogen sources, and Fe salts. The possibility was demonstrated [132] of developing composites based on Co–S and nitrogen-containing CM. Earlier, it was shown [133] that Co_3S_4 is highly active and selective with respect to four-electron reaction of O_2 reduction in 0.1 M KOH. Based on calculations and model concepts, it was assumed [134] that in Co_9S_8, the S^{2-} anions served as the active sites for O_2 adsorption. For preparation of this catalyst, a suspension of Ketjenblack EC-300, PANI (synthesized through aniline oxidation by ammonium peroxydisulfate), and $Co(NO_3)_2$ was treated at 900°C in nitrogen. It was shown that the catalyst composition can be described as Co_9S_8–N–C, where nitrogen is in its quaternary and pyridine forms. The comparison of the above catalytic system with the Fe–N–C and Pt/C catalysts revealed its higher activity as compared with not only the former system but also Pt/C system in the potential region more positive than 0.6 V (RHE). The number of electrons involved in the reaction was ~3.7; Tafel slope was ~0.063 V/decade. However, no information could be found on the further development of this direction.

The characteristics of the catalyst developed by Acta S.p.A (Italy) were studied [135]. This catalyst was synthesized by the pyrolysis of carbon black with the surface of 1400 m^2/g in the mixture of 1.5% Fe + 1.7% Cu in the form of the corresponding phthalocyanines. According to TEM data, the composite consisted of agglomerates with the grain size of 10–30 nm, which corresponded to the specific surface of ~750 m^2/g. High-resolution XPS data revealed no metal particles. Atoms Fe(III) were bound with nitrogen and served as AC, while copper atoms formed a mediator pair Cu(II)/Cu(I) which served for transferring electron from carbon to the $N_xFe(II)O_4H_z$ adduct. Polarization curves demonstrated a well pronounced four-electron wave of O_2 reduction. The activity of FeCu/C at $E > 0.8$ V (RHE) was somewhat lower in 0.1 M KOH than the activity of 30% Pt/C (BASF), but at $E < 0.8$ V (RHE) it exceeded the activity of the platinum catalyst.

Using the liquid-phase method at 90°C, the multicomponent catalysts were synthesized [136] which contained carbon black (Black Pearl 2000), metal (Mn, Fe, Co, Ni, Cu), and polypyrrole. In these catalytic systems, the formation of two types of AC was postulated: $M–N_x$ (where x is 2 or 4) and M=N–C=, which can provide either four- or two-electron reactions. In all the cases, a single polarization wave was observed. As regards selectivity, the catalysts formed the series Mn < Fe < Ni < Cu < Co. Thus, the role of the metal proved to be substantial. The effect of the metal nature on the activity of catalysts synthesized by pyrolysis of pyridine adsorbed on Vulcan XC72 was demonstrated [137]. In systems pyrolyzed at 800°C with the pyridine/carbon black ratio = 40/60, the activity decreased in the row Co > Fe > Ce > W.

Catalysts synthesized by pyrolyzing Co and Fe phthalocyanines and also their mixtures in the 1/1 ratio on Ketjenblack EC-600 carbon black at 600 and 800°C were studied in 0.1 M KOH. In all the cases, a single polarization wave was observed, which was shifted a little to anodic potentials as compared with the Pt/C catalyst [138]. Based on structural studies, the formation of FeCo alloy was concluded. The systems based on two metals, in which carbon black was used as the support and Co phthalocyanine served as the main precursor and which also contained additions of Fe, Co, Ni, V were characterized too [139]. For the pyrolysis temperature of 600°C, the maximum activity was observed for Co–Fe/C catalyst with 40/60 ratio of metals. It was assumed that the AC role was played by the groups of atoms Fe–N and Co–N. For catalysts Me/aminopyrine/BP2000 (700°C), it was shown [140] that the catalytic activity in O_2 reduction in 0.1 M KOH decreased in the row Co ⩾ Fe ~ Cu > Mn ⩾ Ni. The selectivity determined by means of RRDE method changed in the series Fe > Mn > Co ⩾ Cu > Ni. Moreover, the metal-free catalyst aminopyrine/BP2000 (700°C) with the nitrogen content close to that in metal-containing systems exhibited no catalytic activity.

The mixture of starting reagents used in the synthesis of Fe–N–C composite was subjected to mechanochemical treatment [141]. At pH 13, the volume activity of the catalyst in the kinetic-control region (0.8–0.9 V) with Tafel slope of~–0.06 V/decade amounted to 20% of the activity of 46 Pt/C catalyst (TKK).

The authors of ref. [74] have discovered that catalysts with the activity comparable with that of pyrolysis products of metalloporphyrins can also be synthesized based on mixtures of simple compounds, for instance, a mixture of PAN or pyrrole with metal acetates. They also studied the effect of the pyrolysis temperature on the activity of resulting catalysts exhibited in 4 M NaOH at 60°C and placed the optimal pyrolysis temperature in the range of 700–900°C. It was also noted

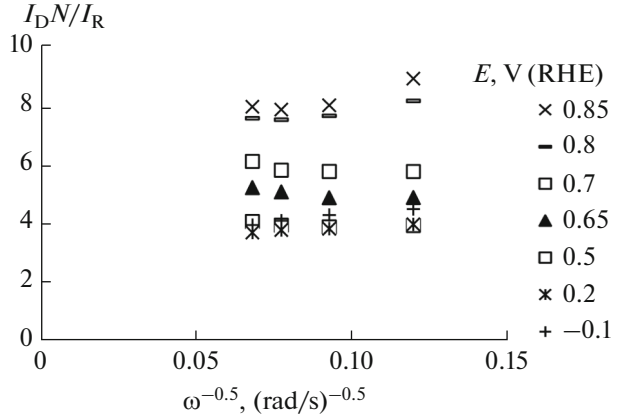

Fig. 10. Dependence I_DN/I_R vs. $\omega^{-0.5}$ for 15% TMPPCo/Vulcan XC72 catalyst treated in 0.5 M H_2SO_4. RRDE, 1 M KOH, 25°C. Collection efficiency $N = 0.25$.

that metal-free products of PAN pyrolysis could be activated by the introduction of cobalt oxides followed by deep cathodic polarization. According to the authors, metal ions formed complex compounds with nitrogen atoms on the electrode surface to produce AC.

It was found [142] that the activity obtained as a result of the mechanical introduction of a carbon support into Co_2O_3/TMPP catalyst after the pyrolysis stage was lower as compared with the case where the support was added before the pyrolysis. According to the authors, this pointed to the key role of carbon during the thermal treatment.

According to the data obtained by RDE and voltammetry [91], the pyrolysis product of 4.4% H_2TMPP/Vulcan XC72 has low activity comparable with that of initial carbon black, in contrast to pyropolymer 4.8% TMPPCo/Vulcan XC72.

The catalytic activity of the catalysts based on the pyrolysis products of the predeposited mixture of Co and Fe complexes with ethylenediamine, synthesized at 800°C did not decrease during cycling in 0.1 M KOH in the potential range of 0.8–1.2 V ($v = 10$ mV/s, 700 cycles), in contrast to its cycling in 0.5 M H_2SO_4 [86]. The activity loss observed in the acidic medium was explained by the degradation of AC associated to pyridine nitrogen atoms. According to XPS data, cycling in the acidic medium resulted in total disappearance of spectrum peaks associated with pyridine ring and pyridine oxide because of their transition to the reduced form, in contrast to alkaline medium. The catalyst stability was studied [143] for the pyrolysis product of poly-TPPFe (at the optimal pyrolysis temperature of 600°C) deposited on Vulcan XC72 carbon black. It was shown that after 10^4 cycles in the potential range from –0.5 to 0.5 V (Hg/HgO/1 M KOH) at the temperature of 20°C, the activity of the poly-TPPFe/Vulcan XC72 catalyst did not decrease. The activity was also retained during 200 cycles of polarization curves of O_2 reduction. In the potentiostatic mode (0.052 V vs. Hg/HgO), the characteristics were observed to decrease by 12% as compared with 31% for the TPPFe/Vulcan XC72 catalyst based on the monomer precursor.

A detailed study of the kinetics and selectivity in oxygen reaction in 0.1 M KOH was carried out by means of RDE and RRDE methods for catalytic systems synthesized by pyrolysis of TMPPCo [109]. By varying the thickness of 30% TMPPCo catalyst layer on RDE from 1.1 to 26.3 μm, it was shown that its macrostructure was accessible to O_2 for the thickness not exceeding 5.3 μm, which corresponded to the catalyst loading of 0.2 mg/cm^2. Varying the amount of TMPPCo from 5 to 30% on Vulcan XC72 has shown that the microstructural accessibility of the surface of catalyst grains is guaranteed for metalloporphyrin amount below 15%. This corresponds to the conditional surface coverage of Vulcan XC72 $\theta < 1.5$. According to the data obtained by means of RRDE method, the catalytic activity as well as the selectivity of the TMPPCo/Vulcan XC72 system containing from 5 to 30% porphyrin with respect to O_2 reduction in 1 M KOH at 60°C depended only insignificantly on the support surface coverage with pyrolysis products. Hence, the increase in the porphyrin content in the catalyst is an inefficient method for enhancing the catalytic properties of the TMPPCo/Vulcan XC72 system. O_2 reduction on the pyrolysis products of TMPPCo proceeded by the parallel path to form the stable products OH^- and HO_2^-. Figure 10 shows that the tangent of the I_DN/I_R vs. $\omega^{-0.5}$ dependence is close to zero.

In contrast to TMPPCo pyropolymers, O_2 reduction on TMPPFeCl pyrolysis products took the parallel-sequential path leading to formation of OH^- and HO_2^- and the further transformation of HO_2^- as follows from the results obtained using RRDE method (Fig. 11) [82]. The selectivity, i.e., k_1/k_2 ratio of the catalyst with 30% TMPPFeCl in 1 M KOH depended, in a complicated manner on the potential, changing from 49 to 19 as the potential varied from 0.9 to 0.2 V (RHE) with the minimum ($k_1/k_2 = 4$) at 0.6 V (RHE). The parallel-sequential path was also taken by the reaction of O_2 reduction in 1 M KOH at 60°C on the products of PAN and 1,1'-diacetylferrocene joint pyrolysis. The selectivity k_1/k_2 decreased in this case from 5.4 to 1.1 as the potential varied from 0.75 to 0.2 V (RHE).

The catalytic activity of CoTMPP/carbon support catalysts and MnO_x–CoTMPP/BP composites was studied in [144]. Comparing CV curves measured in 1 M KOH at 25°C has shown that the catalytic activity of materials synthesized on the carbon black Black Pearl (**BP**) was higher as compared with Vulcan XC72.

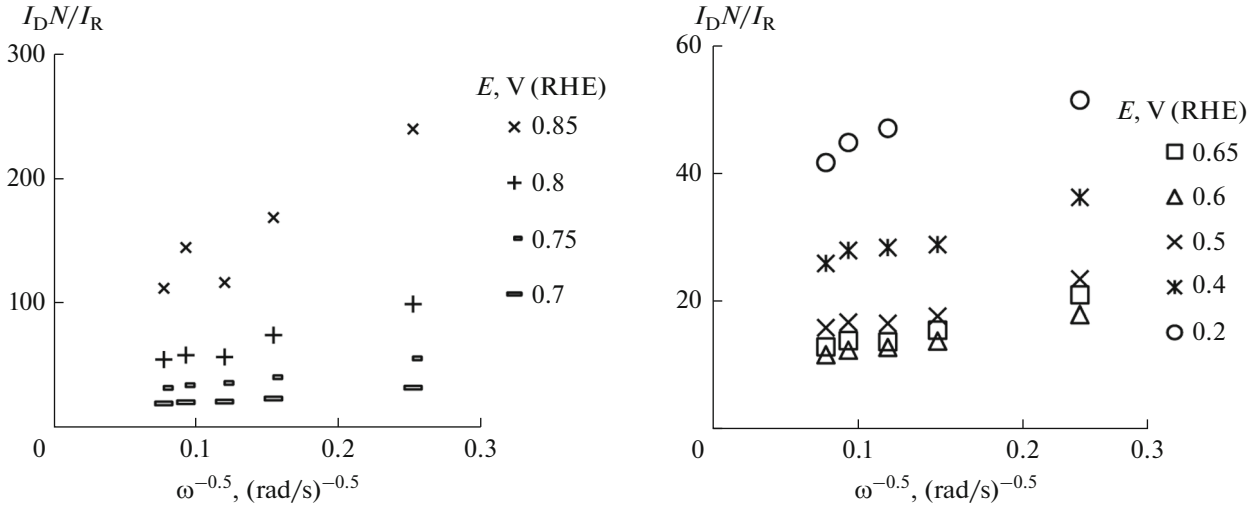

Fig. 11. Dependence I_DN/I_R vs. $\omega^{-0.5}$ for 30% TMPPFeCl/Vulcan XC72 catalyst treated in 0.5 M H_2SO_4. RRDE, 1 M KOH, 25°C. Collection efficiency $N = 0.25$.

Moreover, the preliminary treatment of the support in H_2O_2 solution allowed the catalyst activity to be increased. According to the results obtained on RDE and plotted on the coordinates of Koutecky–Levich equation [144], the number of electrons transferred per O_2 molecule was ~2 for the CoTMPP/BP catalyst.

A CoO/GO(N) catalyst representing a composite containing up to 25% Co in the oxide form was prepared by adsorption of cobalt nitrate on the surface of nitrogenized reduced graphene oxide, which was followed by the thermal treatment at 220°C in inert atmosphere [145]. The nitrogenized reduced graphene oxide was prepared in an autoclave by the hydrothermal treatment (100°C) of reduced graphene oxide in ammonia and hydrazine solution. After nitrogenation, nitrogen content in the material was 4.4 at % according to XPS data. The analysis of results acquired by means of RRDE method in 0.1 M KOH at 25°C has shown that the composite represents a highly active and selective catalyst with onset potential of O_2 reduction of 0.95 V (RHE) at the catalyst loading of 0.6 mg/cm^2 and the half-wave potential of 0.83 V (RHE) at ω = 900 rpm. The yield of H_2O_2 in the potential region of 0.4–0.8 V (RHE) decreased in the following row: Pt/C > CoO/GO(N) > GO(N) > CoO/GO > CoO > GO. At the potential of 0.7 V (RHE), which is of interest for practice, under model conditions (0.1 M KOH at 25°C), for loadings of 0.6 mg/cm^2 for nonplatinum materials and 20 μg_{Pt}/cm^2 for Pt/C, the yield of H_2O_2 (in %) was 0–2 < 3–5 < 7–10 < 12–15 < 20–25 < ~40, respectively. Thus, as follows from the results obtained in ref. [145], the synthesis of composite nonplatinum catalytic systems can be carried out at low temperatures.

In [146], RDE studies of how KOH concentration in the range from 0.05 to 12 M affects O_2 reduction rate and the selectivity were carried on pyridine/Co/Vulcan XC72 composite synthesized at 800°C. The quantity n calculated based on Koutecky–Levich equation decreased insignificantly with the increase in alkali concentration being in average 3.6. In 3 M KOH solution, Tafel slopes for the pyridine/Vulcan XC72 catalyst were ~–0.050 (low polarization region) and ~–0.160 V/decade (high polarization region); for Co/Vulcan XC72, b ~–0.050 and ~–0.230; for pyridine/Co/Vulcan XC72, b ~–0.047 and ~–0.119; and for Pt/C, b ~–0.046 and ~–0.115 mV. The polarization for pyridine/Co/Vulcan XC72 was ~0.150 mV higher as compared with Pt/C.

The effect of KOH solution pH on the peculiarities of O_2 reaction on 30% TMPPCo/Vulcan XC72 catalyst was studied using RDE method [147]. It was shown that as alkali concentration increased, the average number of electrons added to O_2 molecule decreased from 3.4 to 3.0 for E = –0.2 V (RHE) when going from 0.1 M to 4 M KOH.

Thus, the introduction of Co and Fe into the nitrogen–carbon system exerted the clearly distinguishable effect, increasing the activity and forming a single O_2 reduction wave, in contrast to the majority of systems containing no metals. Attempts [147] to use metal atoms other than Co and Fe failed.

For synthesizing catalysts of O_2 reduction to be used in alkaline media, one has to derive a carbon material with incorporated nitrogen atoms and a high specific surface. As a rule, the synthesis is carried out by pyrolysis of C-, N-, and Fe(Co)-containing precursors adsorbed on a dispersed catalytically inactive support, which favors the development of the high

specific surface. The optimal pyrolysis temperature is 800–900°C. The nitrogen atoms can also be incorporated by low-temperature methods. The optimal content of nitrogen atoms is not a universal characteristic as well as the content of metal compounds. Catalysts involving nitrogen and a transition metal of the Fe-group make it possible to carry out oxygen reduction by either parallel-sequential or parallel pathways. In this case, the yield of H_2O_2 as a rule does not exceed 50–60% and, according to available literature data, the reaction selectivity depends little on electrolyte concentration, being, however, determined by the thickness of the catalytic layer and increasing with the increase in the thickness.

4.3. Complex Oxides

Keen attention is drawn to the use of oxide catalysts for O_2 reduction with the structure of spinel ($A_xB_{3-x}O_4$, $0 \leqslant x \leqslant 1$, A = Co, Ni, Li, Mn, Cr, Cu; B = Co, Mn) and perovskite (ABO_3, A = La, Ca, Pr, Sr, Ba; B = Co, Mn, Fe, Ni) and also to the development of gas-diffusion cathodes on their basis to be used in metal–air cells with liquid alkaline electrolytes [6, 7, 148]. In average, the surface of these oxide systems does not exceed 20–50 m^2/g and the cathode thickness reaches 2–3 mm.

Both for manganese (e.g., $Cr_{1-x}Cu_xMn_2O_4$) [149] and cobalt ($Ni_xCo_{3-x}O_4$) [150] spinels, the activity in the reaction of O_2 reduction depends on which cations and in which ratio occupy sites B. The highest activity and stability in 6 M KOH was observed for $MnCo_2O_4$ spinel synthesized on highly dispersed carbon black [151].

The first time that attention was drawn to the activity of perovskites in the reaction of O_2 electroreduction was in ref. [152]. The authors of ref. [153], in a series of publications have shown that in the row of cobaltites, manganites, and ferrites $La_{1-x}A_xBO_3$ (where A is Ca or Sr; B is Co, Fe or Mn) the activity in O_2 reduction decreased ($LaCoO_3 > LaMnO_3 \gg LaFeO_3$), whereas their stability during their operation within AFC increased ($LaCoO_3 \ll LaMnO_3 < LaFeO_3$). This is why, the best way was with La and Mn partialy substituted by Sr and Fe, respectively, to form $La_{1-x}Sr_xMn_{1-y}Fe_yO_3$ starting with manganite $LaMnO_3$. As demonstrated for $La_{0.8}Sr_{0.2}Mn_{1-y}FeyO_3$ (y = 0.0–0.8) and $La_{1-x}Sr_xMn_{0.8}Fe_{0.2}O_3$ (x = 0–0.4), the activity sharply increases with the increase in x and monotonously decreases with the increase in y. For $MeMnO_3$, it was shown [154] that as the ionic radius of the rare-earth metal increased, the catalytic activity of oxides also monotonously increased. The partial substitution of Ca and Sr for La in cobaltites, mangantites, and ferrites was shown [155] to considerably enhance the catalytic activity. It was found in ref. [156] that the catalytic activity of $La_{0.6}Ca_{0.4}CoO_3$ oxide powder with the specific surface of 15 m^2/g in its mechanical mixture with carbon materials decreased in the following series: carbon black Ketjenblack EC-600 (1300 m^2/g) > carbon black Vulcan XC72 (250 m^2/g) > carbon black Vulcan XC72 graphitized at 2700°C and activated at 600°C in air (100 m^2/g) > graphite HS-100 (100 m^2/g) > carbon black Vulcan XC72 graphitized at 2700°C (70 m^2/g). Another way destined to improve the electric contact of the oxide and the current collector is to synthesize highly dispersed particles on the surface of carbon material, as this was done in ref. [151] for oxide of $MnCo_2O_4$ spinel type synthesized by microwave treatment of the respective salts. As the specific surface of the composite catalysts increased above 90 m^2/g, the activity value levels off. This effect was also described earlier in ref. [157] for the active layers based on metalloporphyrin pyrolysis products the composition and the specific surface area of which were dependent on the ratio of two carbon blacks with different degrees of dispersion.

5. THE ACTIVE CENTER STRUCTURE FOR CATALYTIC SYSTEMS, O_2 ADSORPTION AND ACTIVATION, THE SELECTIVITY WITH RESPECT TO O_2 REDUCTION

5.1. Active Centers of Carbon Materials Modified with Nitrogen and Transition Metals

The discussion of the AC structure of nonplatinum systems and the mechanism of electrocatalysis of O_2 reduction should be based on the general principles already known for other catalytic systems which provide acceleration of the reaction and enhance its selectivity. The first of them is the sufficiently strong adsorption of O_2 followed by partial charge transfer to the adsorbed molecule [158]. The second one is protonation of the adsorbed O_2 molecule [158, 159], which provides acceleration of the reaction in acidic solutions in which the transfer of the first electron to O_2 proceeds with the high overpotential as compared with equilibrium potentials of two- and four-electron reactions [8].

In alkaline solutions, the potential values of first-electron transfer for two- and four-electron reactions come closer to one another; and, hence, the reaction of O_2 reduction can proceed at a low adsorption energy even without the adsorption stage [160]. However, under these conditions too, the slow stage is the formation of O_2^- anions which later disproportionate near the electrode. However, the hindered protonation in alkaline electrolytes on platinum metals is accompanied by the decrease in selectivity [117]. Furthermore, in alkaline solutions, the surface coverage with oxygen-containing species (OH_{ads}) [161] that block the AC and complicate the O_2 adsorption increases.

The experimental facts and their interpretation both on the phenomenological level [162, 163] and

based on quantum-chemical calculations [164] made it possible to describe the main peculiarities of O_2 reduction on platinum and compact carbon materials with the low energy of O_2 adsorption [165].

The peculiarities of the AC interaction with the oxygen molecule described above, influencing on the reaction kinetics, its route, and of selectivity, should be used in estimating the efficiency of various types of possible AC in the electrocatalysis of O_2 reduction on nonplatinum systems.

The adsorption energy of molecular oxygen is the most important parameter determining the possibility of the break of the O–O bond and, hence, the selectivity of O_2 reduction. At present, this value was not estimated experimentally for the adsorption of oxygen molecules on AC in electrolyte solutions. The latter fact is general for all the known electrocatalysts of O_2 reduction. The indirect data on the adsorption energy value of O_2 and intermediate species can be calculated in terms of the density functional theory based on some hypothetical AC structures [166]. Hence, in the present stage of studies, the only direct experimental data allowing estimation of the selectivity of O_2 reduction are the results obtained by RRDE method [109, 125]. Within the framework of the theory of parallel-sequential reactions [106], the degree of selectivity of oxygen reduction process is determined by the rate ratio of the direct (with the break of O–O bond) and sequential (through the transient formation of H_2O_2) reactions. Moreover, as was shown above, the mere determination of the yield of hydrogen peroxide [167] or calculation of the number of electrons involved in the reaction according to the Koutecky–Levich equation [73] give no way of obtaining the correct data on the reaction selectivity.

According to theoretical studies [168], the energy of physical adsorption of O_2 on graphite is 0.9 kcal/mol (~3.8 kJ/mol). For nanotubes, the adsorption energy of an oxygen molecule was calculated to be 0.1 eV (9.6 kJ/mol) [169] and 0.25 eV (24.1 kJ/mol) [170]. In this case, the degree of charge transfer from an NT to an O_2 molecule is extremely low, namely, 0.01–0.09 e^-. In alkaline solutions, the additional effect of protonation of the adsorbed oxygen molecule is absent. This fact quite agrees with the available experimental data according to which, irrespective of the CM morphology, i.e., from single-crystal graphite to activated carbons, O_2 reduction in alkaline solutions proceeds only by the sequential mechanism. The close energies for the linear adsorption of O_2 molecule were found in [171] on N- and B-doped CM: 0.3 and 0.5 eV, respectively. Moreover, the dissociation energy of O_2 molecule preliminarily chemisorbed on CM is 0.13 eV.

Of great importance are the results of studying the changes in the electronic and adsorption properties of CM modified with heteroatoms, namely, N, B, S, etc. Quantum chemical calculations have shown [172] that the introduction of heteroatoms into graphene layers increases their basicity and catalytic activity in reactions with electron transfer, e.g., O_2 electroreduction. This approach was developed further in several studies [119, 120, 173] in which systematic investigations of the effect of nitrogen content in NT on their morphology, electronic, and electrochemical properties were carried out in neutral and alkaline electrolytes. According to Raman spectroscopy data, the observed increase in the G/D ratio of band intensities with the increase in the nitrogen content from 0 to 7.4 at % is associated with the increase in the number of defects and edge carbon atoms. According to [174], nitrogen atoms can stabilize the structure defects. The increase in the differential capacitance from 3 to 9 $\mu F/cm^2$ was explained by the formation of a localized donor state near the Fermi level. As the nitrogen content increased, the volume conductivity also increased, and one observed the acceleration of $O_2 + e^- \rightarrow O_2^-$ reaction and the further heterogeneous decomposition of HO_2^-. Thus, the increase in the degree of doping of NT with nitrogen makes their properties closer to those of metals.

In terms of the nanoribbon model and with the use of the density functional theory it was shown that doping with nitrogen of zigzag edges gives rise to the appearance of *n*-conduction. The nitrogen atom has five valence electrons and the neighboring two carbon atoms have valence four. Hence, nitrogen can be considered as the electron donor. The increase in the conduction band occupation shifts it to the valence band [175].

In other studies, attention was focused on peculiarities of the local interaction of O_2 with nitrogen-doped CM. The adsorption of O_2 in the triplet and singlet states on nitrogen-doped NT of various diameters and lengths was considered [68]. The lifetime of adsorbed $^1O_2$ is extremely short; the adsorption of $^3O_2$ in the presence of nitrogen in NT is favorable as regards energy. The electron configuration of $^3O_2$ is similar to that of $^2O_2^-$, and, hence, N-doped NT serve as the effective catalyst of O_2 reduction. The introduction of nitrogen into a NT induces a considerable negative charge, making easier the electron transfer from the nanotube to adsorbed oxygen [176].

The changes in the O–O bond energy at the adsorption on SWNT and N-doped SWNT were calculated for different configurations of the system [177]. For SWNT (10), O_2-dissociation barrier height was found to be 2 eV (192.9 kJ/mol). In the presence of nitrogen in the SWNT structure, in case if O_2 takes the place immediately above nitrogen, the high activation barrier for the molecule dissociation is retained. The alternative configuration is the adsorption interaction with the carbon atoms adjacent to nitrogen

atom. In the latter configuration, the barrier height is observed to decrease to 0.68 eV (65.6 kJ/mol). If nitrogen dopes an NT defect, then the height of the barrier to O_2 dissociation may decrease to 0.03 eV (2.9 kJ/mol). In [178], the concept of the key role played by the carbon atom adjacent to the quaternary nitrogen in the O_2 adsorption and dissociation was elaborated. However, these carbon atoms bear a positive charge, which, according to widely accepted views hardly favors the transfer of negative charge to the oxygen molecule.

In connection with the possibility of the direct reaction of O_2 reduction to water, mention should be made of the studies carried out in acidic solutions in which the protonation of the adsorbed oxygen molecule is possible. Considering OOH as the initial adsorbed species (in strongly acidic solutions), it was concluded [179] that the four-electron reaction is possible after the introduction of nitrogen atom into the system. In the latter case, the AC represents carbon atoms with a high spin density or a high positive charge. In contrast, it was found [83, 180] that irrespective of the nitrogen atom position, i.e., on basal or edge parts, the adsorption energies of O_2 and OOH are too low for the break of the O–O bond, and the reaction proceeds through the formation of H_2O_2.

In the alkaline electrolyte, the protonation of adsorbed O_2 molecules is not discussed. It was assumed [181] that O_{2ads} species are stabilized due to the formation of hydrogen bonds with water molecules. In analogy with protonation, this can favor the acceleration of the stage of first-electron transfer and O_2 dissociation. It was shown that in the absence of water, O_2 cannot be adsorbed on the nitrogen-modified graphene surface. It the presence of water, the chemisorption energy becomes equal to –0.76 eV, and O_{2ads} can be protonated to OOH_{ads} (0.42 eV). Thus, taking account of the energy of stabilization of intermediate species by hydrogen bonds changes the energetics of adsorption of O_2, OOH, O, and OH. According to the authors, the conditions of O_2 reduction in alkaline solutions on quaternary nitrogen are similar to those observed on Pt (111). Moreover, similarly to [182], the slow stage is not the adsorption of O_2 but the removal of O_{ads} or OH_{ads}. In this case, the Tafel slope should correspond to the transfer of the third electron, i.e., be lower than 40 mV per current decade. Such slope is observed only in the initial region of the polarization curve and corresponds to the conditions close to the steady state. However, this assumption contradicts the generally accepted concepts on the kinetics of O_2 reduction with the slow stage of either O_2 adsorption or the transfer of the first electron.

In contrast to acidic solutions, the acceleration of the first-electron transfer to the O_2 molecule in alkaline electrolytes changes the ratio between the stages of first- and second-electron transfer [183]: the inhibition of the second electron transfer at low overvoltages corresponds to the Tafel slope of $\sim 2 \times 2.3RT/3F$ which increases to $\sim 2 \times 2.3RT/F$ at high current densities.

5.2. Active Centers of Complex Oxides

The detailed review [21] devoted to the kinetics and selectivity of O_2 reduction on Co-containing spinels gave no answer on the question of the AC nature and the mechanism of electrocatalytic reduction of O_2. Attention was drawn only to the effect of the nature of cation in the octahedral position and the necessity of the presence in spinel of cations of alternating valence: Co^{2+}/Co^{3+}, Mn^{2+}/Mn^{3+}.

One drawback of spinels, besides their stability [184, 185], is their low selectivity with respect to the four-electron reaction of O_2 reduction. According to [186], the ratio k_1/k_2 for $NiCo_2O_4$ does not exceed 3.5. The cathodic potential shift to 0.6 V decreased the k_1/k_2 ratio to 0.5 [106]. A new method of synthesizing manganese-cobalt spinels on the partly reduced graphene oxide with simultaneous incorporation of nitrogen was proposed [187]. The formation of C–O–metal and C–N–metal bonds was confirmed by spectroscopic data. The activity of such spinel in 0.1 M KOH was not lower than that of 20% Pt/C, and the overall number of electrons involved in the reaction at $E = 0.9$–0.5 V was 4.0–3.8. However, such a complex system can hardly be stable in free concentrated alkaline electrolytes and polymer electrolytes.

One of the first publications in which the oxygen reaction in alkaline solutions was thoroughly studied for a large group of perovskites ABO_3 (A is lanthanum, B is transition metal of the VI–VIII groups) was ref. [188]. It was shown that the mechanisms of reactions of O_2 evolution and reduction are different. The reduction of O_2 proceeds on the surface with the high coverage with OH_{ads} and has the Tafel slope $\sim \frac{RT}{F}$ and the reaction order $\frac{\partial \log i}{\partial \log p_{O_2}} \sim 1$. The presence of *p*-type conduction determines the formation of a space charge in the potential region of the cathodic reaction. Table 2 [189] compares the corrosion and electrochemical properties of certain La-based perovskites. $LaMnO_3$, $LaCoO_3$, and $LaNiO_3$ exhibit high activity but low stability. The introduction of Fe allowed the stability to be increased. The electrochemical activity was measured at $E = -0.160$ V (Hg/HgO), the electrochemical stability was found at $E = -0.260$ V, the chemical stability was assessed by 12-h exposure in 9 N H_2SO_4. The results of chemical and structural analyses of samples are shown by symbols: the presence of La perovskite + peroxide (O), the retention of the perovskite structure (P), the presence of La perovskite + La hydroxide (V), La hydroxide (X).

Table 2. Corrosion and electrochemical properties of perovskites [189]

Oxide	I, mA/cm^2 at $E = -0.160$ V (Hg/HgO)	Electrochemical stability	Chemical stability
$LaMnO_2$	1266	O	O
$LaCoO_3$	1006	X	X
$LaNiO_3$	468	X	O
$LaCrO_3$	344	P	P
$LaFeO_3$	273	P	P
$La_{0.8}SrFeO_2$	519	P	P
$La_{0.6}SrFeCo_{0.4}O_3$	682	V	P
$La_{0.6}Sr_{0.4}Fe_{0,6}Mn_{0.4}O_3$	922	P	P

Table 3. Characteristics of catalytic systems perovskite–carbon black

Composition	Perovskite content, %	Diameter of nanoparticles, nm	i, mA/cm^2 at $E = 0.75$ V
$LaMnO_3$	20	4.1	–
$La_{0.83}Sr_{0.17}MnO_3$	22	4.3	0.6
$La_{0.65}Sr_{0.35}MnO_3$	25	4.4	–
$La_{0.81}Sr_{0.19}MnO_3$	21	7.1	0.53
$La_{0.84}Sr_{0.16}MnO_3$	23	17.6	0.47

The introduction of Ca and Fe into positions A and B, respectively, in $LaMnO_3$ increased the solubility and activity. The introduction of Ca to the A positions increased the activity, because the average valence state of the B position in perovskite lattice increased. $La_{0.4}Ca_{0.6}Mn_{0.6}Fe_{0.4}O_3$, $La_{0.4}Ca_{0.6}CoO_3$, and $La_{0.5}Sr_{0.5}Mn_{0.6}CoO_3$ oxides were studied [150]. Lanthanides $La_{0.6}Sr_{0.4}Fe_{0.8}Mn_{0.2}O_3$ and $La_{0.6}Ca_{0.4}Fe_{0.8}Mn_{0.2}CoO_3$ were found to exhibit adequate activity and stability.

The activity was also observed to increase with the increase in the ionic radius of the rare-earth element in position A. For the most active $PrMnO_3$, the optimal composition was found to be $Pr_{0.6}Ca_{0.4}MnO_3$. The close relationships were observed in [190], where the stability was achieved due to substitution of Ca so that the optimal perovskites were $La_{0.1}Ca_{0.9}MnO_3$ and $La_{0.6}Ca_{0.4}CoO_3$. The low activity of $SrFeMoO_6$ was confirmed [191]. The total substitution of Co for Fe gave rise to the increase in conductivity and activity of oxides, which, however, remained lower as compared with characteristics of Pt/C.

The results of ref. [192] in which a series of $La_{1-x}Sr_xMnO_3$ perovskites with the particle size smaller than 5 nm were synthesized on Ketjen Black carbon black can be considered as successful. Catalytic systems were formed by a modified inverse micelle method [193] (Table 3).

The addition of Sr changed the Mn valence from 3+ to 4+ as a result of occupation of La^{3+} sites by Sr^{2+} ions and also increased the electronic conductivity and made easier the adsorption of O_2 molecules. As follows from Table 3, the decrease in the particle size induced the increase in the current at $E = 0.75$ V on a thin-layer disk electrode. RRDE studies revealed the low yield of peroxide ion in 0.1 M KOH. This pointed to the overall four-electron process of oxygen reduction, although the ratio of the direct and sequential mechanisms was not determined. The potential $E_{1/2}$ for the most active system was 110-mV more negative as compared with 46 Pt/C (TKK) and also 80 mV more positive as compared with 60 Ag/C (BASF).

For $LaCoO_3$ (10 m^2/g) and $La_{0.8}Sr_{0.2}MnO_3$ (17 m^2/g) and also for their composites with Sibunit carbon black (66 m^2/g) containing from 0 to 100 wt % perovskite, it was assumed [194] that carbon black can play the dual role providing the high conductivity and the high degree of catalyst utilization, on the one hand, and initiating the oxygen reduction, on the other hand. Presumably, the activation of O_2 and its reduction to the peroxide anion proceeded on the carbon black surface, while the further transformations of reduction products were provided by the oxide catalyst. The reversibility of redox reactions of perhydroxide anions was studied on the same composite catalysts $LaCoO_3$/carbon black and $La_{0.8}Sr_{0.2}MnO_3$/carbon black [195]. A simplified catalytic model was put

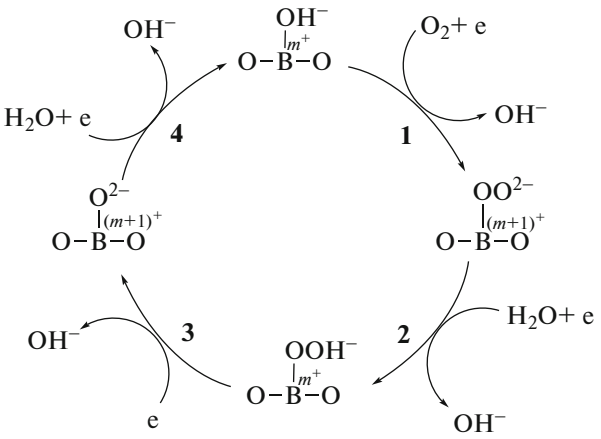

Fig. 12. Hypothetical reaction mechanism of O_2 reduction on perovskites, according to [197].

forward in which it was assumed that the adsorption and reactions of OH_{ads}/O_{ads} proceed on the B^{m+}/B^{m+1} transition-metal cations of ABO_3 perovskites.

The origin of the catalytic activity of perovskites in oxygen reaction was studied in ref. [188, 196]. The authors suggested that the activity of oxide electrodes is determined by the formation and occupation of the σ*-bond between the e_g-orbital of the transition metal and the molecular orbital of adsorbed oxygen. This explanation is similar to that of electrocatalysis of O_2 reduction on platinum-group metals: the closeness of the *d*-band center to the Fermi level [146]. For 15 perovskites it was shown [197] that the key role in acceleration of O_2 reduction is played by the degree of occupation of the σ*-antibonding orbital of the transition-metal atom on the surface. According to this mechanism (see scheme in Fig. 12), the reaction kinetics is limited by the rate of the stage (1) of the O_2^-/OH exchange, i.e., the removal of OH^- species. The rate of this reaction reaches the maximum value at the complete occupation of orbital e_g. Based on the mechanism of O_2 interaction with transition metals proposed in [197], the authors of [198] assumed that the catalytically active species can be both low-spin ions Co^{3+} with the electron configuration t^5e^1 and the high-spin ions Mn^{3+} (t^5e^1) occupying the octahedral positions in $Mn_xCo_{3-x}O_4$ spinels with the mixed cubic-octahedral lattice.

6. STABILITY OF CATALYSTS UNDER MODEL CONDITIONS

The corrosion stability of the carbon support which, for nonplatinum catalysts, represents also the main component of the catalytic system is of no less significance than the electrocatalytic activity. The carbon materials are thermodynamically unstable in the potential region of FC cathode operation, i.e., from 0.5 to 1.0 V (RHE), because the equilibrium potential of their oxidation to CO_2 is 0.207 V under standard conditions. It is only the slow kinetics of carbon oxidation that makes possible its use in oxygen (air) cathodes. In metal–air cells with concentrated alkaline electrolyte at temperature not above 40°C, hydrophobized electrodes of considerable thickness based on activated carbons promoted by pyrolyzed TMPPCo can steadily operate for up to 7–8 thousands of h [199].

The successful operation of electrocatalytic systems in ACPE-based FC puts heavier demands on their corrosion stability, which is associated with the relatively small thickness of electrodes (~10–100 μm), the high concentration of AC and their complex composition. In [200, 201], based on corrosion behavior of CM with different structure, it was proposed to classify CM in two groups with respect to their susceptibility to oxidation. The first group involves disordered carbon, the second one includes graphene-like structures involving packs of graphene monolayers. The relationship between the CM structure and its corrosion stability was also considered [14]. It is well known that graphitization drastically decreases the CM oxidation rate [15]. The corrosion rate is described by the equation $i = kt^{-n}$ [202]. Parameter *k* depends on the temperature and potential, and *n* depends only on the potential. Investigations have shown that the oxidation process can be described under the assumption of the presence of three oxide types on the CM surface: the oxides that reversibly and irreversibly passivate the surface and the catalytically active oxide that produces CO [201].

Doping with nitrogen is an important factor that stabilizes CM [119] by increasing the basicity of this material [84, 203]. The increase in basicity which complicates the surface oxidation is associated with both the delocalization of π-electrons and the properties of nitrogen which is the electron-donor with respect to carbon. This agrees with the conclusions [204] on the enhanced stability of activated carbon after incorporation of nitrogen. In [68], the vertical nitrogen-containing NT were cycled in the interval from +0.2 to –1.2 V (Ag/AgCl) without visible changes in *i* vs. *E* curves up to 100 thousands of cycles. It should also be noted that the activation barrier to the desorption for NO groups is higher as compared with CO groups [205]. In the later studies, the concept of stabilization of carbon supports due to incorporation of nitrogen was considerably developed further for both proton-exchange [29] and anion-exchange [16] electrolytes. In one of the latest studies [206], the oxidized FG samples with the number of layers of 25–35 (80 m^2/g); 12–15 (140 m^2/g), and 5–10 (734 m^2/g) were treated in the NH_3 atmosphere at 700°C for 1–3 h, after which demonstrated good stability in the presence of OH^- ions in the membrane at 150–200°C. It

Table 4. Characteristics of H_2–O_2 (air) FC with ACPE and nonplatinum cathodic catalysts

ACPE type	Cathodic catalyst	t, °C	Gas medium	E_{st}, V	$i_{0.6\ V}$, mA/cm^2	W, mW/cm^2	Reference
A901 Tokuyama Co	46 Pt (TKK 10E50E)/KB	50	H_2/O_2 1 atm	1.06	200	135	[192]
A901 Tokuyama Co	50 Ag (BASF)/Vulcan XC72	50	H_2/O_2 1 atm	–	60	49	[192]
A901 Tokuyama Co	20 $La_{0.83}Sr_{0.17}MnO_3$/KB	50	H_2/O_2 1 atm	0.97	160	129	[192]
A901 Tokuyama Co	46 Pt (TKK 10E50E)/KB 0.4 mg Pt/cm^2	50	H_2/O_2 1 atm	1.04	285	190	[125]
A901 Tokuyama Co	CoFeN/Vulcan XC72 4 mg/cm^2	50	H_2/O_2 1 atm	0.97	285	175	[125]
Commercial membrane + Acta 12 anion-exchange ionomer	Pt/C 0.45 mg/cm^2	46	H_2/air 1 atm	1.05	370	>400	[11]
A901 Tokuyama Co	4020 Acta S.p.A. 0.8 mg/cm^2	46	H_2/air 1 atm	–	260	200	[11]
FAA FuMA-Tech	Co–Fe_3O_4/C	60–80	H_2/O_2 1 atm	0.85	150	114	[207]

was assumed that AC are pyridine groups on the disordered edge structures with the total nitrogen content of ~2.9 at %. In [132], the corrosion stability of systems Pt/C (60 μg/cm^2), FeN/C, and Co_9S_8–N–C in 0.1 M NaOH was studied for potential cycling with the amplitude of 0.2–1.0 V (RHE) up to 5000 cycles. Whereas for Pt/C no changes were observed, the other two systems demonstrated a certain decay in activity in the potential region of limiting diffusion.

The studies devoted to corrosion of CM with different morphology and also of CM modified with other atoms or surface groups are scarce as compared with the importance of the problem of durability of such materials in FC and other devices of electrochemical power engineering. Furthermore, the fundamental questions of CM corrosion such as the kinetics and mechanism of carbon oxidation depending on their structure and the effect of corrosion on the discharge curves were not considered at all.

7. CHARACTERISTICS OF FUEL CELLS WITH ANION-CONDUCTING POLYMER ELECTROLYTE AND NONPLATINUM CATHODE

Cathodic nonplatinum catalysts were used for a long time in the cathodes of metal–air cells with liquid alkaline electrolyte. Certain information on the catalytic systems including oxide, metal- and nitrogen-containing catalysts supported by carbon materials can be found in a review [6]. However, these catalytic systems cannot be used with anion-conducting polymer electrolyte. The catalysts to be used in FC with ACPE should a priori be highly dispersed nanostructures and have the high volume concentration of AC in order to provide the acceptable current densities in active layers of small thickness, because the relatively low conductivity of polymer electrolytes drastically increases the contribution of the ohmic resistance to the overall voltage losses.

Studying both the already known nonplatinum catalysts and/or the catalysts in the stage of development as regards their operation within MEA of H_2–O_2 FC with ACPE makes it possible to compare their characteristics with the analogous ones of the most active monoplatinum catalysts. These studies are scarce so far. Among them, only few demonstrate acceptable current densities, while the data on the stability is virtually absent.

Table 4 demonstrates the characteristics of FC with three types of ACPE (A901 Tokuyama Co [109, 173], Acta 12 [11], and FAA (FuMA-Tech) [207]) and the most efficient nonplatinum cathodic catalysts. For all of them, the MEA surface was 5 cm^2. On the anode, a monoplatinum catalyst was used in all the cases. The data of Table 4 illustrate the comparative tests of MEA with well-known monoplatinum systems on the cathode (46 Pt TKK 10E50E). The highest current densities at 0.6 V and the maximum specific power densities were attained for materials produced by Acta, espe-

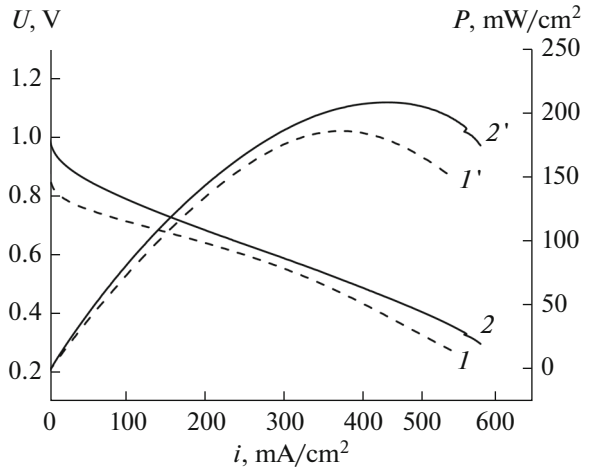

Fig. 13. (*1*, *2*) Voltammograms and (*1'*, *2'*) dependence of the power density on the current density in MEA of H_2–O_2 FC. Membrane Tokuyama A201, ionomer AS-4. cathodic catalysts: (*1*, *1'*) CoFe/Vulcan XC-72, 1 mg_{cat}/cm^2; (*2*, *2'*) 60 wt % Pt/C (HiSPEC9100), 0.4 mg_{Pt}/cm^2. Anodic catalyst 60 wt % Pt/C (HiSPEC9100), 1 mg_{Pt}/cm^2. 50°C, without excessive pressure.

cially as these tests, in contrast to the others, employed air as the oxidant instead of oxygen. However, the commercial membrane used by the authors is unknown. In [92, 125], the membrane and ionomer produced by Tokuyama were used. The highest current densities at the voltage of 0.6 V (~300 mA/cm^2) and the maximum power density (~180 mW/cm^2) were reached in [125]. Moreover, the MEA performance remained virtually unchanged upon substitution of 4 mg/cm^2 of the CoFeN/Vulcan XC72 composite for 0.4 mg/cm^2 of Pt, but the open-circuit voltage decreased from 1.04 to 0.97 V. Other types of ACPE and nonplatinum cathodic catalysts are also used for ACPE-based FC (e.g., [208]). However, the characteristics achieved in these studies are far below those shown in Table 4.

H_2–O_2 FC comprising FAA (FuMA-Tech) anion-exchange membrane, the cathodic metal-free catalyst N-800 based on the pyrolysis product of supported carbamide, and 40% Pt/C (E-TEK, 0.5 mg/cm^2) as the anode catalyst was tested [209]. For the gas pressure of 1 atm and the temperature of 50°C, the specific power value of 30 mW/cm^2 was reached.

With the exception of ref. [11], the data on the durability of ACPE-based FC or of the cathodic catalyst used in these FC are not available. It is merely known that CO_2-unscrubbed air could be used with Acta 12 ionomer with certain performance degradation.

In Frumkin Institute of Physical Chemistry and Electrochemistry of the Russian Academy of Sciences, we carried out the studies on developing and optimizing of H_2-air FC on the basis of A-4 ionomer, A901 membrane and either supported platinum or nonplatinum cathodic catalysts with different types of carbon supports and Fe/Co precursors. The obtained data will be published in a special paper; here we show the highlights (Fig. 13) characterizing the difference in the discharge curves for FC with cathodes based on Pt/C and nonplatinum catalytic systems.

8. CHALLENGES AND PROSPECTS OF INVESTIGATIONS IN THE FIELD OF NONPLATINUM CATALYSTS FOR ALKALINE FUEL CELLS

The interest in studies of catalysis of molecular oxygen electrochemical reduction does not wear out for decades and will grow further due to the demands for the development of crucial electrochemical power engineering technologies. Research and development of nanosized nonplatinum electrocatalysts for alkaline media, stimulated by the modern applied problems of reducing the cost and size of power sources with concurrent increase in their performance, is to be continued. The studies in this direction are stimulated by certain achievements in the field of development of anion-conducting polymer electrolytes. The targeted development of nanosized nonplatinum catalysts for fuel cells with anion-exchange membranes is indicated by the fact that the model studies of materials are carried out in dilute alkaline solutions (e.g., 0.1 M KOH) with pH close to that of the polymer anion-conducting electrolyte. It should be reminded that for fuel cells with liquid electrolyte and metal–air cells, the catalysts are usually tested in concentrated alkaline solutions with the alkali concentration of 1–8 M.

Unfortunately, at present, a weak correlation is observed between the experimental results obtained under model conditions and those of the catalysts testing within membrane-electrode assemblies of FC with ACPE. Up to date, there are few data available on the prototype tests of ACPE- and nonplatinum cathodes-based FC. The only correct estimation of catalysts' practical relevance is their direct application on the cathodes of FC prototypes. Furthermore, the correct assessment of the catalytic properties is possible only under model conditions.

Currently, to make an assessment of the available experimental data and to lay down the main challenges to the development of platinum-free anion-exchange membrane fuel cells, the following conclusion can be drawn. First, there are no data on the performance of membrane-electrode assemblies of fuel cells with metal-free catalysts as the cathode materials. Second, more attention should be paid to studying the corrosion properties of catalysts under model conditions and their degradation within fuel cells. Third, the development of practically applicable anodic nonplatinum catalysts is at the very beginning. It is the development of such catalysts that will allow taking advantage of the chief potential virtue of fuel cells with

anion-exchange membrane as compared with those based on proton-exchange membranes, namely, the total absence of platinum. Fourth, the already available results of H_2–O_2 fuel cells tests show the closeness of the characteristics of monoplatinum and nonplatinum cathodes, the fact which argues for carrying on further investigations to step-by-step handling of existing problems, overcoming the difficulties and experimental contradictions mentioned above.

The experimental and, especially, theoretical studies point to the possibility of developing selective catalysts for molecular oxygen reduction to OH^- on the basis of N-doped metal-free carbon materials. Their advantage is the relatively high corrosion resistance due to the presence of nitrogen atoms. Cathodic catalysts of this group are potentially the most promising for FC with ACPE.

LIST OF ABBREVIATIONS

AC	active center
AcC	activated carbon
ACPE	anion-conducting polymer electrolyte
AFC	alkaline fuel cell
BET	method of Brunauer–Emmett–Teller
CM	carbon material
CV	cyclic voltammetry
DES	density of electron states
ECG	electrochemical generator
EDL	electric double layer
FC	fuel cell
FG	few-layer graphene
GO	graphene oxide
HOG	highly oriented graphite
NT	nanotubes
NW	nanowires
PAN	polyacrylonitrile
PANI	polyaniline
PEM	proton-exchange membrane
PP	polypyrrole
RDE	rotating disk electrode
RRDE	rotating ring-disk electrode
TC	turbostratic carbon
TMPPCo	cobalt tetramethoxyphenylporphyrin
TMPPFeCl	iron tetramethoxyphenylporphyrin chloride

ACKNOWLEDGEMENTS

This study was carried out with the finacial support from the Russian Foundation for Basic Research, project no. 13-0300317.

REFERENCES

1. Borup, R., Meyers, J., Pivovar, B., Kim, Y.S., Mukundan, R., Garland, N., Myers, D., Wilson, M., Garzon, F., Wood, D., Zelenay, P., More, K., Stroh, K., Boncella, J., McGrath, J.E., Inaba, et al., *Chem. Rev.*, 2007, vol. 107, p. 3904.
2. Perry, M.L. and Fuller, T.F., *J. Electrochem. Soc.*, 2002, vol. 149, p. 59.
3. *"Kvant": energiya pobedy* ("Kvant": Energy of Victory), Moscow: MAKD, 2009, p. 184.
4. Gülzow, E., *Fuel cells,* 2004, vol. 4, p. 251.
5. Bidault, F. and Kucernak, A., *J. Power Sources,* 2010, vol. 195, p. 2549.
6. Neburchilov, V., Wang, H., Martin, J.J., and Qu, W., *J. Power Sources*, 2010, vol. 195, p. 1271.
7. Bidault, F., Brett, D.J.L., Middleton, P.H., and Brandon, N.P., *J. Power Sources,* 2009, vol. 187, p. 39.
8. Tarasevich, M.R., *Russ. J. Electrochem.,* 2013, vol. 49, p. 600.
9. Merle, G. and Wessling, M., *J. Membr. Sci.*, 2011, vol. 377, p. 1.
10. Varcoe, J.R. and Slade, R.C.T., *Fuel cells,* 2005, vol. 5, p. 187.
11. Piana, M., Boccia, M., Filpi, A., Flammia, E., Miller, H.A., Orsini, M., Salusti, F., Santiccioli, S., Ciardelli, F., and Pucci, A., *J. Power Sources,* 2010, vol. 195, p. 5875.
12. Santasalo-Aarnio, A., Hietala, S., and Kallio, T., *J. Power Sources,* 2011, vol. 196, p. 6153.
13. Radovic, L.R. and Rodriguez-Reinoso, F., in *Chemistry and Physics of Carbon,* vol. 25, New York: Marcel Dekker, 1997, p. 243.
14. Tarasevich, M.R., *Elektrokhimiya uglerodnykh materialov* (Electrochemistry of Carbon Materials), Moscow: Nauka, 1984.
15. Kinoshita, K., *Carbon: Electrochemical and Physicochemical Properties,* New York: Wiley, 1988.
16. Liu, G., Li, X., Ganesan, P., and Popov, B.N., *Electrochim. Acta,* 2010, vol. 55, p. 2853.
17. McClure, J.P., Thornton, J.D., Jiang, R., Chu, D., Cuomo, J.J., and Fedkiw, P.S., *J. Electrochem. Soc.,* 2012, vol. 159, p. F733.
18. Tarasevich, M.R., Radyushkina, K.A., and Bogdanovskaya, V.A., *Elektrokhimiya porfirinov* (Electrochemistry of Porphyrins), Moscow: Nauka, 1991.
19. Dodelet, J.P., *N4-Macrocyclic Metal Complexes: Electrocatalysis, Electrophotochemistry and Biomimetic Electroanalysis*, New York: Springer Science and Business Media, 2006.
20. Tarasevich, M.R. and Efremov, B.N., in *Electrodes of Conductive Metallic Oxides*, Amsterdam: Elsevier, 1980, p. 221.
21. Hamdani, M., Singh, R.N., and Chartier, P., *Int. J. Electrochem. Sci.*, 2010, vol. 5, p. 556.
22. Marsh, H. and Rodriguez-Reinoso, F., *Activated Carbon*. Elsevier, 2006.
23. *Proizvodstvo i svoistva uglerodnykh sazh. Nauch. trudy VNII sazhevaya promyshlennost'* (Production and Properties of Carbon Blacks. Transactions of the

Research Institute of Carbon Black Industry), Omsk, 1972, no. 1, p. 320.

24. D'yachkov, P.N., *Uglerodnye nanotrubki: stroenie, svoistva, primeneniya* (Carbon nanotubes Structure, Properties, Applications), Moscow: BINOM. Laboratoriya znanii, 2006.
25. Kuzov, A.V., Lozovaya, O.V., and Tarasevich, M.R., *Al'tern. Energ. Ekol.*, 2012, no. 2 (106), p. 114.
26. Yin, S., Mu, S., Pan, M., and Fu, Z., *J. Power Sources,* 2011, vol. 196, p. 7931.
27. Lian, J., Zheng, Y., Chen, J., Liu, J., Hulicova-Jurcakova, D., Jaroniec, M., and Qiao, S.Z., *Angew. Chem., Int. Ed. Engl.,* 2012, vol. 51, p. 3892.
28. Wood, T.E., Tan, Z., Schmoeckel, A.K., O'Neill, D., and Atanasoski, R., *J. Power Sources*, 2008, vol. 178, p. 510.
29. Olson, T.S., Dameron, A.A., Wood, K., Pylypenko, S., Hurst, K.E., Christensen, S., Bult, J.B., Ginley, D.S., O'Hayre, R., Dinh, H., and Gennett, T., *J. Electrochem. Soc.,* 2013, vol. 160, p. F389.
30. Charreteur, F., Ruggeri, S., Jaouen, F., and Dodelet, J.P., *Electrochim. Acta,* 2008, vol. 53, p. 6881.
31. Wu, L., Nabae, Y., Kuroki, S., Kakimoto, M., and Miyata, S., *ECS Trans.,* 2011, vol. 41, p. 2313.
32. Lefevre, M. and Dodelet, J.-P., *ECS Trans.*, 2012, vol. 45, p. 35.
33. Trogadas, P., Fuller, T.F., and Strasser, P., *Carbon,* 2014, vol. 75, p. 5.
34. Ma, T.-Y., Liu, L., and Yuan, Z.-Y., *Chem. Soc. Rev.,* 2013, vol. 42, p. 3977.
35. Herrmann, I., Kramm, U.I., Fiechter, S., and Bogdanoff, P., *Electrochim. Acta,* 2009, vol. 54, p. 4275.
36. Jaouen, F., Herranz, J., Lefevre, M., Dodelet, J.P., Kramm, U.I., Herrmann, I., Bogdanoff, P., Maruyama, J., Garsuch, A., Dahn, J.R., Pylypenko, S., Atanassov, P., and Ustinov, E.A., *ACS Appl. Mater. Interfaces*, 2009, vol. 1, p. 1623.
37. Krivenko, A.G. and Komarova, N.S., *Russ. Chem. Rev.,* 2008, vol. 77, p. 927.
38. Sun, Y., Wu, Q., and Shi, G., *Energy Environ. Sci,* 2011, vol. 4, p. 1113.
39. Pumera, M., *Energy Environ. Sci,* 2011, vol. 4, p. 668.
40. Brownson, D.A.C., Kampouris, D.K. and Banks, C.E., *J. Power Sources,* 2011, vol. 196, p. 4873.
41. Park, H.J., Meyer, J., Roth, S., and Skakalova, V., *Carbon,* 2010, vol. 48, p. 1088.
42. McCreery, R.L., *Chem. Rev.,* 2008, vol. 108, p. 2646.
43. Fujimoto, H., Mabuchi, A., Tokumitsu, K., and Akuzawa, N., *Carbon*, 1994, vol. 32, p. 193.
44. Randin, J.-P. and Yeager, E., *J. Electroanal. Chem.*, 1972, vol. 36, p. 257.
45. Xia, J., Chen, F., Li, J., and Tao, N., *Nat. Nanotechnol.*, 2009, vol. 4, p. 505.
46. Geim, A.K. and Novoselov, K.S., *Nat. Mater.*, 2007, vol. 6, p. 183.
47. Soto, G., Samano, E.C., Machorro, R., Castillion, F.F., Farias, M.H., and Cota-Araiza, L., *Superficies Vacio,* 2002, vol. 15, p. 34.
48. Zhou, J.-K., Sui, Z.-J., Zhu, J., Li, P., Chen, D., Dai, Y.-C., and Yuan, W.-K., *Carbon,* 2007, vol. 45, p. 785.
49. Sljukis, B., Banks, C.E., and Compton, R.G., *J. Iran. Chem. Soc,* 2005, vol. 2, p. 1.
50. Soboleva, T., Zhao, X., Malek, K., Xie, Z., and Holdcroft, S., *ACS Appl. Mater. Interfaces,* 2010, vol. 2, p. 375.
51. Lefevre, M. and Dodelet, J.P., *Electrochim. Acta,* 2008, vol. 53, p. 8269.
52. Tarasevich, M.R., Bogdanovskaya, V.A., Lozovaya, O.V., Maleeva, E.A., and Kol'tsova, E.M., *Al'tern. Energ. Ekol.,* 2012, no. 1(105), p. 82.
53. Chan, K. and Eikerling, M., *J. Electrochem. Soc.,* 2011, vol. 158, p. B18.
54. Yang, Z., Nie, H., Chen, X., Chen, X., and Huang, S., *J. Power Sources,* 2013, vol. 235, p. 238.
55. Sun, Y., Li, C., and Shi, G., *J. Mater. Chem.,* 2012, vol. 22, p. 12810.
56. Zhou, X., Yang, Z., Nie, H., Yao, Z., Zhang, L., and Huang, S., *J. Power Sources,* 2011, vol. 196, p. 9970.
57. Sheng, Z.-H., Shao, L., Chen, J.-J., Bao, W.-J., Wang, F.-B., and Xia, X.-H., *ACS Nano,* 2011, vol. 5, p. 4350.
58. Liang, J., Zheng, Y., Chen, J., Liu, J., Hulicova-Jurcakova, D., Jaroniec, M., and Qiao, S.Z., *Angew. Chem., Int. Ed. Engl.,* 2012, vol. 51, p. 3892.
59. Gavrilov, N., Pašti, I.A., Mitrić, M., Travas-Sejsić, J., Ćirić-Marjanović, G., and Mentus, S.V., *J. Power Sources,* 2012, vol. 220, p. 306.
60. Vikkisk, M., Kruusenberg, I., Joost, U., Shulga, E., Kink, I., and Tammeveski, K., *Appl. Catal. B: Environ.*, 2014, vol. 147, p. 369.
61. Xu, P., Wu, D., Wan, L., and Liu, R., *J. Colloid Interface Sci.,* 2014, vol. 421, p. 160.
62. Liu, R., Wu, D., Feng, X., and Mullen, K., *Angew. Chem., Int. Ed. Engl.,* 2010, vol. 49, p. 2565.
63. Vujković, M., Gavrilov, N., Pašti, I., Krstić, J., Travas-Sejdić, J., Ćirić-Marjanović, G., and Mentus, S., *Carbon,* 2013, vol. 64, p. 472.
64. Yang, D.-S., Chaunhari, S., Rajesh, K.P., and Yu, J.-S., *Chem. Cat. Chem.,* 2014, vol. 6, p. 1236.
65. Nam, G.,Park, J., Kim, S.T., Shin, D., Park, N., Kim, Y., Lee, J.-S., and Chao, J., *Nano Lett.,* 2014, vol. 14, p. 1870.
66. Geng, D., Ding, N., Liu, Z., Sun, X., and Zong, Y., *J. Mater. Chem. A,* 2015, vol. 3, p. 1795.
67. Alexeyeva, N., Shulga, E., Kisand, V., Kink, I., and Tammeveski, K., *J. Electroanal. Chem.,* 2010, p. 169.
68. Gong, K., Du, F., Xia, Z., Durstock, M., and Dai, L., *Science,* 2009, vol. 323, p. 760.
69. Wang, L. and Pumera, M., *J. Power Sources,* 2014, vol. 50, p. 12662.
70. Liu, J., Jiang, L., Tang, Q., Wang, E., Qi, L., Wang, S., and Sun, G., *Appl. Catal. B*, 2014, vol. 148-149, p. 212.
71. Davydova, E.S., *Russ. J. Electrochem.,* 2013, vol. 49, p. 733.
72. Bron, M., Fiechter, S., Hilgendorff, M., and Bogdanoff, P., *J. Appl. Electrochem.,* 2002, vol. 32, p. 211.

73. Liu, G. and Popov, B.N., *J. Power Sources,* 2010, vol. 195, p. 6373.
74. Gupta, S., Tryk, D., Bae, I., Aldred, W., and Yeager, E., *J. Appl. Electrochem.,* 1989, vol. 19, p. 19.
75. Ferrandon, M., Kropf, A.J., Myers, D.J., Artyushkova, K., Kramm, U., Bogdanoff, P., Wu, G., Johnston, C.M., and Zelenay, P., *J. Phys. Chem.,* 2012, vol. 116, p. 16001.
76. Bashyam, R. and Zelenay, P., *Nature,* 2006, vol. 443, no. 7, p. 63.
77. Meng, H., Larouche, N., Lefevre, M., Jaouen, F., and Dodelet, J.-P., *Electrochim. Acta,* 2010, vol. 55, p. 6450.
78. Kramm, U.I., Herrmann-Geppert, I., Bogdanoff, P., and Fiechter, S., *J. Phys. Chem.,* vol. 47, p. 23417.
79. Bruser, V., Savastenko, N., Schmuhl, A., Junge, H., Herrmann, I., Bogdanoff, P., and Schroder, K., *Polym.,* 2007, vol. 4, p. 94.
80. Matter, P.H., Wang, E., and Ozkan, U.S., *J. Catal.,* 2006, vol. 243, p. 395.
81. Jeong, B., Uhm, S., and Lee, J., *ECS Trans.,* 2010, vol. 33, p. 1757.
82. Davydova, E.C., *Cand. Sci. (Chem) Dissertation*, Moscow, 2014.
83. Sidik, R.A., Subramanian, N.P., Kumaraguru, S.P., and Popov, B.N., *J. Phys. Chem. B,* 2006, vol. 110, p. 1787.
84. Strelko, V.V., Karte, N.T., Dukhno, I.N., Kuts, V.S., Clarkson, R.B., and Odintsov, B.M., *Surf. Sci.,* 2004, vol. 548, p. 281.
85. Biddinger, E.J. and Ozkan, U.S., *J. Phys. Chem. C,* 2010, vol. 114, p. 15306.
86. Liu, G., Li, X., Lee, J.-W., and Popov, B.N., *Catal. Sci. Technol.*, 2011, vol. 1, p. 207.
87. Jaouen, F. and Dodelet, J.-P., *Electrochim. Acta,* 2007, vol. 52, p. 5975.
88. Matter, P.H. and Ozkan, U.S., *Catal. Lett.,* 2006, vol. 109, p. 115.
89. Contamin, O., Debiemme-Chouvy, C., Savy, M., and Scarbeck, G., *J. New Mater. Electrochem. Syst.*, 2000, vol. 3, p. 67.
90. Gojkovic, S.L., Gupta, S., and Savinell, R.F., *J. Electrochem. Soc.,* 1998, vol. 145, p. 3493.
91. Scherson, D.A., Gupta, S.L., Fierro, C., and Yeager, E.B., *Electrochim. Acta,* 1983, vol. 28, p. 1205.
92. Bacon, F.T., *Electrochim. Acta,* 1969, vol. 14, p. 569.
93. Hamdani, M., Singh, R.N., and Chartier, P., *Int. J. Electrochem. Sci,* 2010, vol. 5, p. 556.
94. Roche, I., Chainet, E., Chatenet, M., and Vondrdk, J., *J. Appl. Electrochem.*, 2008, vol. 38, p. 1195.
95. Mazin, P.V., Kapustina, N.A., Kleimenov, B.V., and Tarasevich, M.R., *Al'tern. Energ. Ekol.*, 2010, no. 3, p. 44.
96. Shaskol'skaya, M.P., *Kristallografiya* (Crystallography), Moscow: Vyssh. shk, 1984.
97. *Perovskite Oxide for Solid Oxide Fuel Cells*, Ed. Ishihara, T. N.Y.: Springer Science + Business Media, Inc., 2009.
98. Efremov, B.N. and Tarasevich, M.R., *Elektrokhimiya,* 1981, vol. 17, p. 1672.
99. King, W.J. and Tseung, A.C.C., *Electrochim. Acta,* 1974, vol. 19, p. 485.
100. Lukasiewicz, J.P., Imaizumi, S., Yuasa, M., Shimanoe, K., and Yamazoe, N., *J. Mater. Sci.,* 2006, vol. 41, p. 6215.
101. Lavela, P., Tirado, J.L., and Vidal-Abarca, C., *Electrochim. Acta*, 2007, vol. 52, p. 7986.
102. Rojas, R.M., Vila, E., and Garcia, O., Martin de Vidales, J.L., *J. Mater. Chem.,* 1994, vol. 4, p. 1635.
103. Cheng, F., Shen, J., Peng, B., Pan, Y., Tao, Z., and Chen, J., *Nat. Chem,* 2011, vol. 3, p. 79.
104. Lamminen, J., Kivisaari, J., Lampinen, M.J., Viitanen, M., and Vuorisalo, J., *J. Electrochem. Soc.,* 1991, vol. 138, p. 905.
105. Yuasa, M., Shimanoe, K., Teraoka, Y., and Yamazoe, N., *Solid-State Lett.,* 2011, vol. 14, p. A67.
106. Tarasevich, M.R., Khrushcheva, E.I., and Filinovskii, V.Yu., *Vrashchayushchiisya diskovyi elektrod s kol'tsom* (Rotating Ring-Disk Electrode), Moscow: Nauka, 1987.
107. Frumkin, A.N. and Aikazyan, E.A., *Dokl. Akad. Nauk SSSR*, 1955, vol. 100, p. 315.
108. Koutetskii, Ya. and Levich, V.G., *Zh. Fiz. Khim.,* 1958, vol. 32, p. 1565.
109. Davydova, E.S. and Tarasevich, M.R., *Prot. Met. Phys. Chem. Surf.,* 2015, vol. 51, p. 240.
110. Tsivadze, A.Yu., Tarasevich, M.R., Bogdanovskaya, V.A., and Kapustina, N.A., *Dokl. Phys. Chem.,* 2008, vol. 420, part 2, p. 154.
111. Sugawara, M., Ohno, M., and Matsuki, K., *J. Mater. Chem.,* 1997, vol. 7, no. (5), p. 833.
112. Paliteiro, C. and Correia, E., *Portug. Electrochim. Acta*, 2006, vol. 24, p. 83.
113. Restovic, A., Rios, E., Barbato, S., Ortiz, J., and Gautier, J.L., *J. Electroanal. Chem.,* 2002, vol. 522, p. 141.
114. Biddinger, E.J., von Deak, D., Singh, D., Marsh, K., Knapke, D.S., and Ozkan, U.S., *J. Electrochem. Soc.,* 2011, vol. 158, p. B402.
115. Zhutaeva, G.V., Bogdanovskaya, V.A., Davydova, E.S., Kazanskii, L.P., and Tarasevich, M.R., *J. Solid State Electrochem.,* 2014, vol. 18, p. 1319.
116. Gasteiger, H.A., Kocha, S.S., Sompalli, B., and Wagner, F.T., *Appl. Catal. B*, 2005, vol. 56, p. 9.
117. Tarasevich, M.R. and Khrushcheva, E.I., *Kinetika slozhnykh elektrokhimicheskikh reaktsii* (Kinetics of Complex Electrochemical Reactions) Moscow: Nauka, 1981.
118. Liang, H.-W., Wu, Z.-Y., Chen, L.-F., Li, C., and Yu, S.-H., *Nano Energy,* 2015, vol. 11, p. 366.
119. Maldonado, S. and Stevenson, K.J., *J. Phys. Chem. B*, 2005, vol. 109, p. 4707.
120. Wiggins-Camacho, J.D. and Stevenson, K.J., *J. Phys. Chem. C,* 2009, vol. 113, p. 19082.
121. Geng, D., Liu, H., Chen, Y., Li, R., Sun, X., Ye, S., and Knights, S., *J. Power Sources,* 2011, vol. 196, p. 1795.
122. Chen, Z., Higgins, D., and Chen, Z., *Electrochim. Acta,* 2010, vol. 55, p. 4799.

123. Lia, H. and Cheng, X., *224th ECS Meeting, San Francisco, California,* 2013, no. 1567.
124. Vazquez-Arenas, J., Higgins, D., Chen, Z., Fowler, M., and Chen, Z., *J. Power Sources,* 2012, vol. 205, p. 215.
125. Li, X., Popov, B.N., Kawahara, T., and Yanagi, H., *J. Power Sources,* 2011, vol. 196, p. 1717.
126. Li, X., Liu, L., Lee, J.-W., and Popov, B.N., *J. Power Sources,* 2008, vol. 182, p. 18.
127. Shi, J., Xu, P., Zhen, M.F., and Qiao, J., *224th ECS Meeting, San Francisco, California,* 2013, no. 1378.
128. Lee, S.U., Belosludov, R.V., Mizuseki, H., and Kawazoe, Y., *Small,* 2009, vol. 5, p. 1769.
129. Kramm, U.I., Herranz, J., Larouche, N., Arruda, T.M., Lefevre, M., Jaouen, F., Bogdanoff, P., Fiechter, S., Abs-Wurmbach, I., Mukeriee, S., and Dodelet, J.-P., *Phys. Chem. Chem. Phys.,* 2012, vol. 14, p. 11673.
130. Wu, G., More, K.L., Xu, P., Wang, H.-L., Ferrandon, M., Kropf, A.J., Myers, D.J., Ma, S., and Zelenay, P., *Chem. Commun.,* 2013, vol. 49, p. 3291.
131. Wu, G., Li, Q., and Zelenay, P., *224th ECS Meeting, San Francisco, California,* 2013, no. 1566.
132. Wu, G., Chung, H., Nelson, M., Artyushkova, K., More, K.L., and Zelenay, P., *ECS Trans.,* 2011, vol. 41, p. 1709.
133. Okamoto, Y., Nakano, H., Imanaka, T., and Teranishi, S., *Bull. Chem. Soc. Jpn*., 1975, vol. 48, p. 1163.
134. Sidik, R.A. and Anderson, A.B., *J. Phys. Chem. B,* 2006, vol. 10, p. 936.
135. He, Q., Yang, X., Ren, X., Koel, B.E., Ramaswamy, N., Mukerjee, S., and Kostecki, R., *J. Power Sources,* 2011, vol. 196, p. 7404.
136. Lia, Z.P., Liu, Z.X., Zhu, K.N., Li, Z., and Liu, B.N., *J. Power Sources,* 2012, vol. 219, p. 163.
137. Qiao, J., Ding, L., Xu, L., Dai, X., and Liu, Y., *ECS Trans.,* 2012, vol. 45, p. 111.
138. Bambagioni, V., Bianchini, C., Filippi, J., Lavacchi, A., Oberhauser, W., Marchionni, A., Moneti, S., Vizza, F., Psaro, R., Dal, SantoV., Gallo, A., Recchia, S., and Sordelli, L., *J. Power Sources,* 2011, vol. 196, p. 2519.
139. Ding, L., Dai, X., Lin, R., Wans, H., and Qiao, J., *J. Electrochem. Soc.,* 2012, vol. 159, p. F577.
140. Xu, P., Chen, W., Wang, Q., Wu, M., Qiao, J., Chen, Z., and Zhang, J., *RSC Adv,* 2015, vol. 5, p. 6195.
141. Meng, H., Jaouen, F., Proietti, E., Lefevre, M., and Dodelet, J.-P., *Electrochem. Commun.,* 2009, vol. 11, p. 1986.
142. Mocchi, C. and Trasatti, S., *J. Molecular Catal. A,* 2003, vol. 204-205, p. 713.
143. Xu, S., Li, Z., Ji, Y., Wang, S., Yin, X., and Wang, Y., *Int. J. Hydr. Energy,* 2014, vol. 39, p. 20171.
144. Xie, X.-Y., Ma, Z-F., Ma, X-X., Ren, Q., Schmidt, V.M., and Huang, L., *J. Electrochem. Soc.,* 2007, vol. 154, p. B733.
145. He, Q., Li, Q., Khene, S., Ren, X., Lopez-Suarez, F.E., Lozano-Castello, D., Bueno-Lopez, A., and Wu, G., *Phys. Chem. C*, 2013, vol. 117, p. 8697.
146. Qiag, J., Xua, L., Liu, Y., Xu, P., Shi, J., Liu, S., and Tian, B., *Electrochim. Acta*, 2013, vol. 96, p. 298.
147. Qing, X., Shi, J., Xu, P., and Qiao, J., *224th ECS Meeting, San Francisco, California,* 2013, no. 1535.
148. Egan, D.R., Ponce de Leon, C., Wood, R.J.K., Jones, R.L., Stokes, K.R., and Walsh, F.C., *J. Power Sources,* 2013, vol. 236, p. 293.
149. Ortiz, J. and Gautier, J.L., *J. Electroanal. Chem.,* 1995, vol. 391, p. 111.
150. Ponce, J., Rehspringer, J.-L., Poillerat, G., and Gautier, J.L., *Electrochim. Acta,* 2001, vol. 46, p. 3373.
151. Nissinen, T.A., Kiros, Y., Gasik, M., and Leskela, M., *Chem. Mater.,* 2003, vol. 15, p. 4974.
152. Meadowcroft, D.B., *Nature (London),* 1970, vol. 226, p. 847.
153. Hyodo, T., Hayashi, M., Mitsutake, S., Miura, N., and Yamazoe, N., *J. Appl. Electrochem.,* 1997, vol. 27, p. 745.
154. Hyodo, T., Hayashi, M., Mitsutake, S., Miura, N., and Yamazoe, N., *J. Electrochem. Soc.,* 1996, vol. 143, p. L266.
155. Hayashi, M., Uemura, H., Shimano, K., Miura, N., and Yamazoe, N., *J. Electrochem. Soc.,* 2004, vol. 151, p. A158.
156. Muller, S., Holzer, F., Arai, H., and Haas, O., *J. New Mater. Electrochem. Syst.,* 1999, vol. 2, p. 227.
157. Kiros, Y. and Schartz, S., *J. Power Sources,* 1991, vol. 36, p. 547.
158. Sidik, R.A. and Anderson, A.B., *J. Electroanal. Chem.,* 2002, vol. 528, p. 69.
159. Andersen, A.B., Cai, Y., Sidik, R.A., and Kan, D.A., *J. Electroanal. Chem.,* 2005, vol. 580, p. 17.
160. Yang, H.H. and McGreery, R.L., *J. Electrochem. Soc.,* 2000, vol. 147, p. 3420.
161. Ramaswamy, N. and Mukerjee, S., *ECS Trans.,* 2010, vol. 33, p. 1777.
162. Tarasevich, M.P., *Elektrokhimiya,* 1981, vol. 17, p. 1208.
163. Sepa, D.B., Vojnovic, M.V., and Damjanovic, A., *Electrochim. Acta,* 1981, vol. 26, p. 781.
164. Nørskov, J.K., Rossmeisl, J., Logadottir, A., Lindvist, L., Kitchin, J.R., Bligaard, T., and Jensson, H., *J. Phys. Chem. B*, 2004, vol. 108, p. 17886.
165. Tarasevich, M.R., Sabirov, F., and Burshtein, R.Kh., *Elektrokhimiya,* 1971, vol. 7, p. 404.
166. Kattel, S., Atanassov, P., and Kiefer, B., *Phys. Chem. Chem. Phys.,* 2013, vol. 15, p. 148.
167. Brocato, S., Serov, A., and Atanassov, P., *Electrochim. Acta,* 2013, vol. 87, p. 361.
168. Sovscu, D.C., Jorda, K.D., and Avouris, P., *J. Phys. Chem. B,* 2001, vol. 105, p. 11227.
169. Peng, S. and Cho, K., *Nanotecnology,* 2000, vol. 11, p. 57.
170. Jhi, S.-H., Louie, S.G., and Cohe, M.L., *Phys. Rev. Lett.,* 2000, vol. 85, p. 1710.
171. Flyagina, I.S., Hughes, K.J., Pourkashanian, M., and Ingham, D.B., *Fuel Cells,* 2014, vol. 14, p. 709.
172. Strelko, V.V., Kuts, V.S., and Thrower, P.A., *Carbon,* 2000, vol. 38, p. 1499.
173. Maldonado, S., Morin, S., and Stevenson, K.J., *Carbon,* 2006, vol. 44, p. 1429.
174. Kattel, S.P., Kiefer, B., and Atanassov, P., *ECS Trans.,* 2010, vol. 33, p. 551.
175. Huang, B., *Phys. Lett. A,* 2011, vol. 375, p. 845.

176. Hu, X., Wu, Y., Li, H., and Zhang, Z., *J. Phys. Chem. C,* 2010, vol. 11, p. 9603.

177. Shan, B. and Cho, K., *Chem. Phys. Lett.,* 2010, vol. 492, p. 131.

178. Kiuchi, H., Kondo, T., Sakurai, M., Niwa, H., Miyawaki, J., Harada, Y., Ikeda, T., Hou, Z., Terakura, K., Nakamura, J., and Oshima, M., *224th ECS Meeting, San Francisco, California,* 2013, no. 1493.

179. Zhang, L. and Xia, Z., *J. Phys. Chem.,* 2011, vol. 115, p. 11170.

180. Kurak, K.A. and Anderson, A.B., *J. Phys. Chem. C,* 2009, vol. 113, p. 6730.

181. Yu, L., Pan, X., Cao, X., Hu, P., and Bao, X., *J. Catalysis,* 2011, vol. 282, p. 183.

182. Nilekar, A.U. and Mavrikakis, M., *Surf. Sci.,* 2008, vol. 602, p. L89.

183. Appleby, A.J. and Marie, J., *Electrochim. Acta,* 1979, vol. 24, p. 195.

184. Gautier, J.L., Marco, J.F., Gratia, M., Gancedo, J.R., de la Garza Guadarrama, V., Nguyen-Cong, K., and Chartier, P., *Electrochim. Acta,* 2002, vol. 48, p. 119.

185. Singh, R.N., Lai, B., and Malviya, M., *Electrochim. Acta,* 2004, vol. 49, p. 4605.

186. Heller-Ling, N., Prestat, M., Gautier, J.-L., Koenig, J.-F., Poillerat, G., and Chartier, P., *Electrochim. Acta,* 1997, vol. 42, p. 197.

187. Liang, Y., Wang, H., Zhou, J., Li, Y., Wans, J., Resier, T., and Dai, H., *J. Am. Chem. Soc.,* 2012, vol. 134, p. 3517.

188. Bockris, J.O. and Otagawa, T., *J. Phys. Chem.,* 1983, vol. 87, p. 2960.

189. Hyodo, T., Shimizu, Y., Miura, N., and Yamazoe, N., *Denki Kagaku,* 1994, vol. 62, p. 158.

190. Bursell, M., Pirjamali, M., and Kiros, Y., *Electrochim. Acta,* 2002, vol. 47, p. 1651.

191. Cheriti, M., Kahoul, A., Azizi, A., and Alonso-Vante, N., *Ionics,* 2013, vol. 19, p. 1155.

192. Saito, M., Takakuwa, T., Kenko, T., Daimon, K., Tasaka, A., Inaba, M., Shiroishi, K., Hatai, T., and Kuwano, J., *ECS Trans.,* 2013, vol. 58, p. 1335.

193. Inaba, M., Tasaka, A., Saito, M., Takakuwa, T., and Kenko, T., Japan Patent 2012-041242, 2012.

194. Poux, T.T., Napolskiy, F.S., Dintzer, T., Kerangueven, G., Istomin, S.Ya., Tsirlina, G.A., Antipov, E.V., and Savinova, E.R., *Catal. Today,* 2012, vol. 189, p. 83.

195. Poux, T., Bonnefont, A., Ryabova, A., Kerangueven, G., Tsirlina, G.A., and Savinova, E.R., *Phys. Chem. Chem. Phys.,* 2014, vol. 16, p. 13595.

196. Matsumoto, Y., Yoneyama, H., and Tamura, H., *J. Electroanal. Chem.,* 1977, vol. 79, p. 319.

197. Suntivich, J., Gasteiger, H.A., Yabuuchi, N., Nakanishi, H., Goodenough, J., and Shao-Horn, Y., *Nat. Chem.,* 2011, vol. 3, p. 546.

198. Lee, E., Jang, J.-K., and Kwon, Y.-U., *J. Power Sources*, 2015, vol. 273, p. 735.

199. Gamburzev, S., Iliev, I., and Kaisheva, A., *2nd Conf. "Electrochemical Power Sources". Zilina, CSSR*, 1981, p. 25.

200. Gallasher, K.G. and Fuller, T.F. *Phys. Chem. Chem. Phys.*, 2009, vol. 11, p. 11557.

201. Gallagher, K.G., Yushinb, G., and Fuller, T.F., *J. Electrochem. Soc.,* 2010, vol. 157, p. B820.

202. Kinoshita, K. and Bett, J., *Carbon,* 1973, vol. 11, p. 237.

203. Biniak, S., Szymanski, G., Siedlewski, J., and Swiatkowski, A., *Carbon,* 1997, vol. 35, p. 1799.

204. Mang, D., Boehm, H.P., Stanczyk, K., and Marsh, H., *Carbon,* 1992, vol. 30, p. 391.

205. Montoya A., Gil J.O., Mondragon F., and Truong T.N., *Prepr. Symp. - Am. Chem. Soc., Div. Fuel Chem.,* 2002. V. 47. P. 424.

206. Hibino, T., Kobayashi, K., and Heo, P., *Electrochim. Acta,* 2013, vol. 112, p. 82.

207. Wang, C.-H., Lin, Y.-C., Chang, S.-T., and Chang, S.L.Y., *J. Power Sources,* 2015, vol. 277, p. 147.

208. Hu, Q., Li, G., Pan, J., Tan, L., Lu, J., and Zhuang, L., *Int. J. Hydrogen Energy,* 2013, vol. 38, p. 16264.

209. Unni, S.M., Bhange, S.N., Illathvalappil, R., Mutneja, N., Patil, K.R., and Kurungot, S., *Small,* 2015, vol. 11, p. 352.

Translated by T. Safonova